Evolution process of the Late Silurian–Late Devonian tectonic environment in Qimantagh in the western portion of east Kunlun, China: Evidence from the geochronology and geochemistry of granitoids

Nana Hao[1], Wanming Yuan[1,*], Aikui Zhang[2], Yunlei Feng[1], Jianhui Cao[1], Xiaoning Chen[1], Xueqin Cheng[1] and Xuanxue Mo[1]

[1]*China University of Geosciences, No. 29, Xueyuan Road, Beijing 100083, People's Republic of China.*
[2]*Qinghai No. 3 Geology and Prospecting Institution, Xining 810019, China.*
[*]*Corresponding author. e-mail: ywm010@sina.com*

The East Kunlun Orogenic Belt has undergone a composite orogenic process consisting of multiple orogenic cycles and involving many types of magmatic rocks spread over the whole district. However, due to bad natural geographical conditions and complex superimposed orogenic processes, most of the Caledonian orogenic traces were modified by the late tectonic uplift and denudation, so these rocks are poorly studied. Multiperiodic magmatic activity during the Late Silurian (approximately 420 Ma)–Late Devonian (approximately 380 Ma) exists in the Qimantagh area. We obtained 5 zircon U–Pb ages from the Late Silurian–Late Devonian granitoids in the Qimantagh area. Those ages are 420.6 ± 2.6 Ma (Nalingguole biotite monzogranite), 421.2 ± 1.9 Ma (Wulanwuzhuer potassium granite), 403.7 ± 2.9 Ma (Yemaquan granodiorite), 391.3 ± 3.2 Ma (Qunli granite porphyry), and 380.52 ± 0.92 Ma (Kayakedengtage granodiorite). These granitoids belong to the sub-alkaline, high-K calc-alkaline, metaluminous or weakly or strongly peraluminous series. The rocks are right oblique types, having overall relative LREE enrichment and HREE depletion, though rocks from different times may exhibit different degrees of Eu anomalies or overall moderate Eu depletion. The rocks are rich in large ion lithophile elements (LILE), such as Rb, Th, and K, and high field strength elements (HFSE), such as Zr and Hf, and are depleted in Ba, Nb, Ta, Sr, P, Eu, and Ti. The rocks have complex composition sources. The Late Silurian granitoids are mainly crust-derived. Most of the Devonian granitoids are crust-mantle mixed-source and only some parts of them are crust-derived, especially the Middle Devonian granitoids. Those mid-acidic and acidic intrusive rocks are formed in a post-collision tectonic setting, lithosphere delamination may have occurred in the Early Devonian (407 Ma), and the study area subsequently experienced an underplating of the mantle-derived magma at least until the Late Devonian (380 Ma).

1. Introduction

The East Kunlun Orogenic Belt (EKOB) is a long (5000 km) tectonic belt across Mainland China and is a giant magmatic belt equivalent to the Gangdise belt in the Tibetan Plateau (Mo *et al.* 2007). The EKOB is located in the Northern Qinghai–Tibet Plateau, bounded by the Qaidam Basin to the north (Cheng 1994; Wang *et al.* 1990) and belonging to the western part of Mainland China's central orogenic belt (Jiang 1992; Jiang *et al.* 2000; Yin *et al.* 1999; Liu *et al.* 2003) across the Paleo-Asian

Keywords. Tectonic evolution; zircon U–Pb dating; geochemistry; granitoid; Late Silurian–Late Devonian; Qimantagh.

and Tethys tectonic domains. The belt has undergone a composite orogenic process consisting of multiple stages and cycles over several eras, such as the Early Paleozoic Caledonian cycle and the Late Paleozoic–Early Mesozoic Hercynian–Indosinian cycle. The plate subduction and collision in different periods have left their traces on this area (Jiang 1992; Pan *et al.* 1996; Yin and Zhang 1997, 1998; Zhu *et al.* 1999, 2005; Yang *et al.* 2009). Magmatic rocks of various types and ages are spread over the whole district, and the Caledonian and Variscan–Indosinian tectonic-magmatic activity is significant here. Previous research on the Variscan–Indosinian granites is relatively abundant, but due to the bad natural geographical conditions and the complex superimposed orogenic process, most of the Caledonian orogenic traces were modified by the late tectonic uplift and denudation, and are not well preserved, so these traces are poorly studied.

In recent years, many geologists (Bai *et al.* 2004; Wang *et al.* 2004; Zhao *et al.* 2008; Guo *et al.* 2011; Tan *et al.* 2011; Wang 2011) found multiple Late Silurian–Late Devonian granitoids in the Qimantagh region in the western part of the East Kunlun Mountains and researched their geochemical characteristics and tectonic environment. However, they never performed a specific and detailed discussion about the evolution process of the tectonic environment during this period. We have carried out detailed geological field studies, and with the help of systematic geochemistry and LA-ICP-MS zircon geochronological age data, confirmed that mid-acidic and acidic granitoids existed during the Late Silurian (approximately 420 Ma)–Late Devonian (approximately 380 Ma). Hence, we contribute to a beneficial discussion about the geological tectonic environment and evolution of the area providing more detailed information on the early Paleozoic orogenic cycle of the Qimantagh area, laying a foundation towards understanding the tectonic evolution of the EKOB and providing a basis for the Proto-Tethys Ocean changing into the Paleo-Tethys Ocean.

2. Geological setting

The EKOB is bounded by the Qaidam basin to the north, the Bayan Har-Songpan Ganzi block to the south, the Qinling–Dabie orogenic belt to the east and the NE-trending Altyn Tagh Fault to the west (figure 1a). The belt has the feature of north–south dissimilitude and west–east differentiation on regional geologic structures. The northern, central, and southern Kunlun faults (Huang *et al.* 1977, 1984; Jiang *et al.* 1994; Qu *et al.* 1994; Yang 1994; Cao *et al.* 1999) divide the Kunlun region into three distinct zones from north to south (Yuan *et al.* 2000), while Wutumeiren serves as the boundary between the western (Qimantagh area) and eastern (Dulan area) segments of the EKOB.

Qimantagh, across all of its geological tectonic units from north to south, is the widest and most exposed orogenic belt of the EKOB. According to Pan's (2002) classification scheme, it is composed of five major tectonic units from north to south (figure 1a): the Qaidam continental block (I1), the northern early Paleozoic magmatic arc and junction belt of the Qimantagh (I2), the Kunlun block (I3), the South Kunlun subduction–collision complex rock zone (I4), and the Yulong–Bayankala marginal foreland basin (II1). There are also five important deep faults in the region corresponding to each unit: the Golmud buried fault (F5, the northern branch of the northern Kunlun fault), the Adatan fault (F4), the Nalingguole river fault (F3, the southern branch of the southern Kunlun fault), the central Kunlun fault (F2), and the southern Kunlun fault (F1).

The research of this article includes only the Qimantagh area, which is limited to the north of the central Kunlun fault (F2), the east of Yaziquan, and the west of Wutumeiren across multiple tectonic belts. Tectonic activities in the study area are well developed, and the main faults are F5, F4, F3, and F2 (figure 1a). These faults have obvious control significance to the regional tectonic-magmatic activity. The magma activity of the Qimantagh area is noticeably strong and has characteristics from multiple eras corresponding to four orogenic cycles: Precambrian (Proterozoic), Early Paleozoic ($\in$–D_3), Late Paleozoic–Early Mesozoic (D_3–T_3), and Late Mesozoic–Cenozoic (after Early Jurassic). The magmatic activity happened mainly during the Caledonian, Variscan, and Indosinian–Yanshan orogenies. The distribution of magmatic rocks, especially mid-acidic and acidic intrusive rocks, is very extensive, and the rock types include mainly granodiorite-monzonitic granite-moyite. The distribution of the pluton (long axis direction), controlled by regional tectonics, is to the north–west, which is consistent with regional tectonic lines (figure 1b). The strata outcropped in the study area are relatively complete and range from Archean to Cenozoic in age. The strata mainly include the following: Changcheng Period, Jinshuikou Group intermediate-deep metamorphic rocks; Jixian Period, Langyashan Group shallow metamorphic carbonates mingling with clastic rocks; upper and middle Ordovician shallow metamorphic clastic rocks mingling with a small amount of altered ultrabasic rocks; upper Devonian sandy conglomerates and volcanic rocks; Carboniferous carbonates and fine clastic rocks; lower Triassic carbonates and thinly layered siltstones; upper Triassic continental intermediate-acid volcanic series;

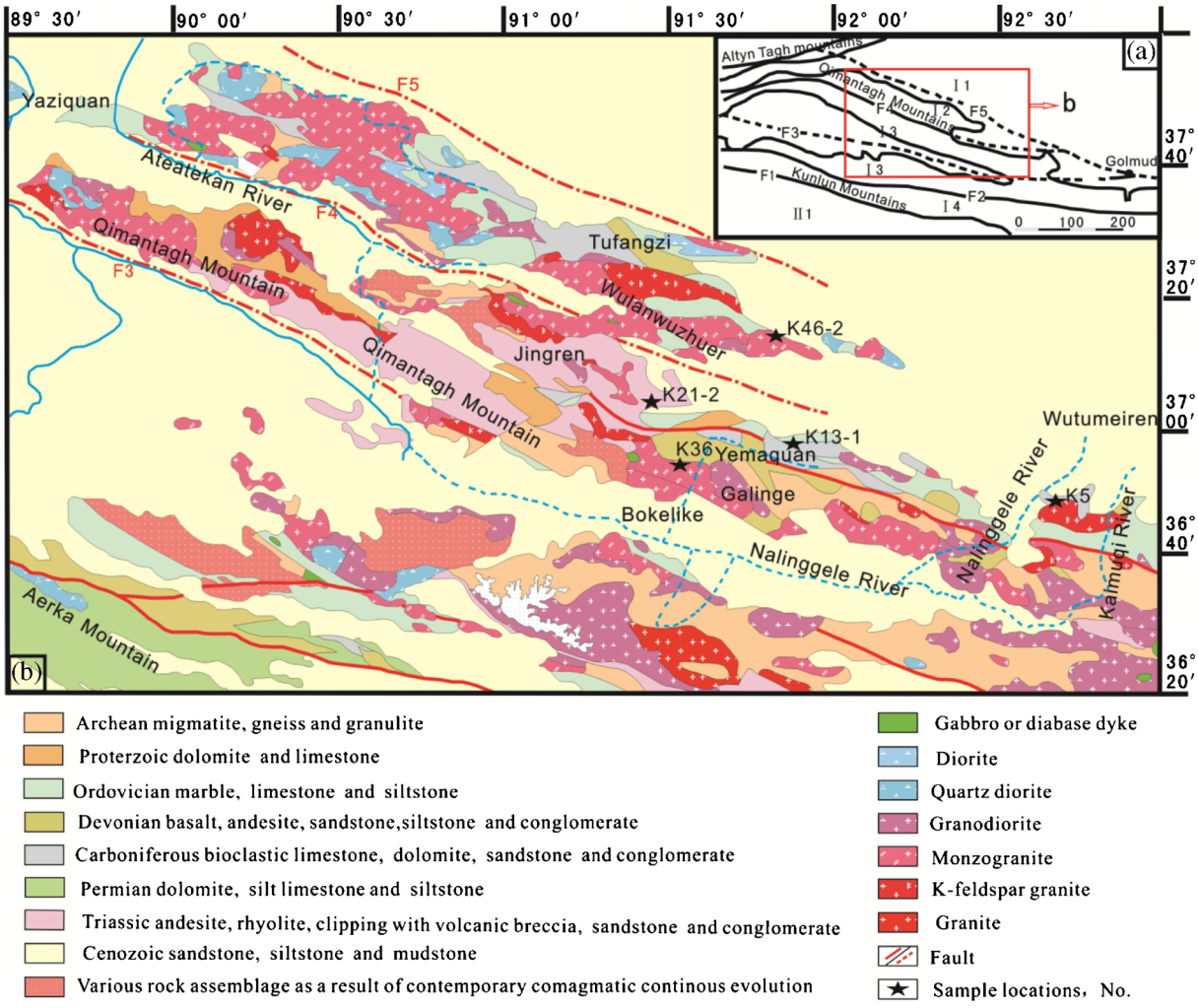

Figure 1. Geological sketch map of intrusive rocks in Qimantagh area, East Kunlun Mountains.

and Cenozoic continental sandy conglomerates, siltstones and some loose accumulation.

The tectonic evolution of the EKOB underwent four orogenic cycles. A metamorphic crystalline basement formed in the Paleoproterozoic, and the tectonic environment belonged to a passive continental margin environment in the Mesoproterozoic–Neoproterozoic. The ancient Qaidam land collided with the micro-landmass of central Kunlun in the Late Neoproterozoic, while the EKOB formed under a wide range of events in the Cambrian–Ordovician, forming many ocean basins, such as the central Kunlun ocean basin and the northern side of the slightly smaller Qimantagh ocean basin. Ocean basins within the eastern segment of the EKOB formed and expanded towards the end of the Neoproterozoic and the Middle Cambrian, and subduction lasted from the Middle Cambrian to the Late Ordovician. The ocean basins had completely closed by the Late Silurian–Middle Devonian and subsequently experienced the principal collision–post-collision orogenic stages (Mo *et al.* 2007). The slight difference between the western and eastern segments of the EKOB is that the western segment of the central Kunlun Ocean subducted towards the north in the Late Ordovician to the Early Silurian, while the Qimantagh Ocean subducted from north to south. The ocean basin completely closed in the Early Silurian (the closing time is slightly earlier than that of the eastern segment), and the development of the continental molasse formation in the Late Devonian marks the end of the early Paleozoic orogenic cycle (at present, there is no unified theory of when the Qaidam block and the central Kunlun continent collided or when the study area turned into a post-collision environment). After the early Paleozoic orogenic cycle, the regional Paleo-Asian Ocean began converging from west to east (Xiao *et al.* 1990), while the Paleo-Tethys Ocean of the southern EKOB underwent extension (Fang and Liu 1996). The south Kunlun ocean basin in the EKOB formed in the Early Permian, inferring that the south Kunlun ocean basin began opening in the Early Carboniferous. The small, previously closed central Kunlun ocean

basin opened once again and became the marginal sea or back-arc basin in the eastern segment of the EKOB. The EKOB was in the major subduction orogenic period in the Middle–Late Permian to Early Triassic (240–260 Ma), when the southern Kunlun ocean subducted towards the north, and entered the collision–post-collision intracontinental orogenic stage in the Late Triassic. The EKOB experienced lithosphere delamination (Gao and Jin 1997; Be'dard 2006; Chen *et al.* 2005) and an underplating of mantle-derived magmas at the end of the Late Triassic to the Early Jurassic, which resulted in the formation of the Qaidam basin (Mo *et al.* 2007). Following the Late Paleozoic–Mesozoic orogenic stage, the Tethys tectonic domain transferred into the Neo-Tethys tectonic evolution stage, and the subjected position of the Neo-Tethys also moved southward to the Bangong Nujiang and Yarlung Zangbo Suture Zones. In the Late Mesozoic–Cenozoic, East Kunlun only experienced remote effects, mainly displaying the formation and development of the thrust structure system, the shortening level of the continental crust, the formation and evolution of the Qaidam basin, and the strong uplift of the East Kunlun Mountains (Mo *et al.* 2007).

3. Sample descriptions

Five representative plutons were selected and 5 samples corresponding to each pluton in the Qimantagh were collected. The details are as follows.

Most of the Nalingguole pluton is covered by Quaternary sediments, so there are few exposed outcrops. The rock types of this pluton are primarily monzonitic granite; for example, sample K5 (biotite monzonitic granite) is located to the east of the Nalingguole River, and the latitude, longitude, and height of the sample are 92°51.585′E, 36°48.309′N, and 3191 m, respectively. Biotite monzonitic granite is grey to off-white in colour with a medium-fine granular texture and massive structure, consisting mainly of quartz (approximately 25%), plagioclase (approximately 30%), K-feldspar (approximately 30%), biotite (approximately 10%), hornblende (approximately 5%), and accessory minerals including titanite, magnetite, apatite and zircon. In figure 2(a and b), the following are observed: the quartz possesses a subhedral–anhedral texture and exhibits wavy extinction; the plagioclase displays multiple twins; the centre of the K-feldspar exhibits kaolinisation; the dark brown to brown biotite shows chloritisation and opaque iron materials; and the light green hornblende displays a band structure, two groups of diamond cleavage and simple twins.

The Yemaquan granodiorite pluton has only sparse exposure. Sample K13-1 (GPS: 92°00.654′E, 36°58.939′N, height: 3707 m) was collected from drill core ZK10033. It is off-white in colour with a medium-fine granitic texture and massive structure. The main minerals are subhedral–anhedral quartz (approximately 30%), plagioclase (approximately 40%), and potassium feldspar (approximately 20%). The secondary minerals are biotite and hornblende (total approximately 10%), and the accessory minerals are mainly zircon, apatite, magnetite, and ilmenite. In figure 2(c and d), we can see that kaolinisation has occurred in the plagioclase and K-feldspar, so the surfaces are dirty. The biotite has partly turned into pennine and presents an indigo interference colour, and the yellow-green hornblende, which has developed a simple twin, has an interference colour of level 3 blue.

Granite porphyry (K21-2) in the Qunli mine was collected from borehole ZK1701, and it is off-white to light reddish in colour with a medium grain porphyritic structure and massive structure. In figure 2(e and f), it can be seen that the phenocrysts and the matrix mainly consist of quartz, K-feldspar and seldom biotite. Some quartz phenocrysts have euhedral crystals, while some were corroded into harbour by the matrix. The potassium feldspar phenocrysts exhibit kaolinisation, so the surface is dirty. The biotite phenocryst has developed a dark rim due to alteration.

The Kayakedengtage complex, located in the southeastern Qimantagh Mountain, is a batholith, and the exposed area covers approximately 386 km^2. The distribution direction of the complex is in the WNW–ESE direction, and the long axis direction roughly parallels the Nalingguole river fault (F3). The complex has multiple types of rocks, mainly consisting of gabbro, diorite, quartz diorite, granodiorite, monzonitic granite and syenogranite, which are products of a typical magmatic mixing process (Chen *et al.* 2006). The monzonitic granite and granodiorite are the main rock types, and their exposed areas are 218 and 83 km^2, respectively. We collected one sample (K36) of the Kayakedengtage complex in the field, and the specific location of sample K36 (granodiorite) is 91°39.075′E, 36°56.232′N with a height of 4409 m. The rock is off-white in colour with medium-fine granitic texture and massive structure. The main minerals are quartz (approximately 30%), plagioclase (approximately 40%), and potassium feldspar (approximately 20%). The secondary minerals are biotite and hornblende (total approximately 10%), and the accessory minerals are mainly zircon and apatite. In figure 2(g and h), the plagioclase contains long and short columnar crystals, multiple twins and carbonation. The K-feldspar has Carlsbad twins, while some alkali-feldspars are

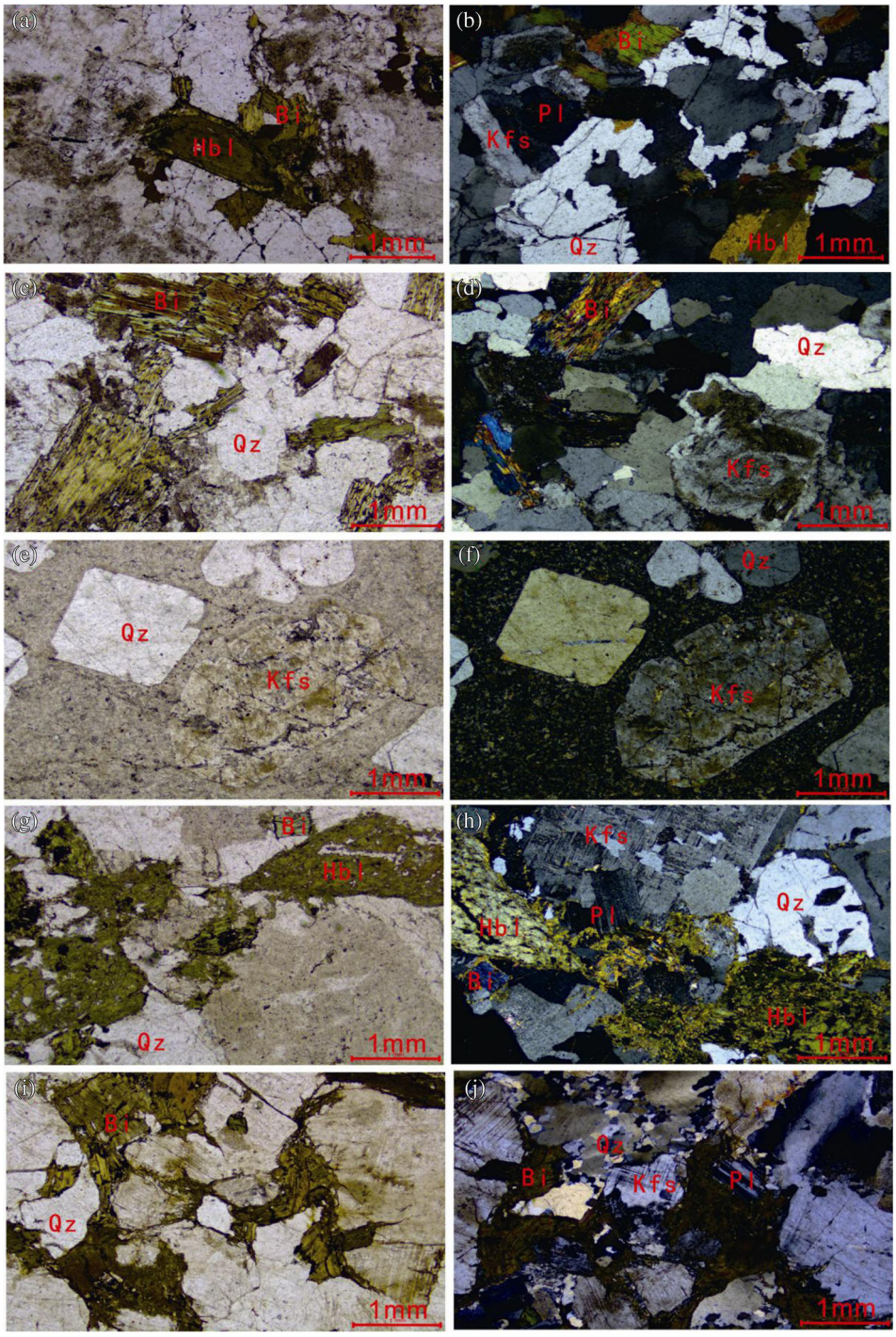

Figure 2. Petrographic characteristics of granites in Qimantagh area. Abbreviations: Qtz: quartz; Pl: plagioclase; Kfs: potassic feldspar; Hbl: hornblende; Bi: biotite.

microcline with lattice twins. The dark brown biotite has partly turned into pennine and presents an indigo interference colour, whereas the yellow-green hornblende has developed diamond cleavage and has an interference colour of level 3 blue.

The Wulanwuzhuer pluton body has an irregular shape, but because it was affected by the later tectonic and erosion, it is even more complex. The overall distribution direction of the body is towards the northwest. The rock association of this pluton is primary granodiorite-monzogranite-potassium granite. We collected one sample (K46-2) of the Wulanwuzhuer pluton in the field, and the location of sample K46-2 (potassium granite) is 91°54.198′E, 37°14.968′N. The rock is reddish in colour with a medium-fine granular texture and massive structure. In figure 2(i and j), quartz (approximately 25%), potassium feldspar (approximately 45%),

and plagioclase (approximately 20%) are the major mineral components, while biotite and hornblende (total approximately 10%) are the secondary minerals and zircon and apatite are the main accessory minerals. There are two stages of quartz: the early quartz is larger and irregularly shaped, while the later particles are smaller and are distributed around the gap between the larger quartz and feldspar. The K-feldspar has Carlsbad twins, and the minority of alkali-feldspar is microcline with lattice twins. Generally, the biotite irregularly fills the gap between the potassium feldspar and quartz.

4. Analytical methods

4.1 *Zircon U–Pb geochronology*

Representative samples for zircon separation are selected according to standard procedures, followed by mechanical crushing and magnetic and electromagnetic analyses. Pure zircon grains were handpicked using a binocular microscope, and together with several grains of standard zircon TEMORA, they were mounted onto an epoxy resin disc and ground down so that their interiors were exposed and polished. After preparing the mount, the zircons were first photographed by optical microscopy, and then cathodoluminescence (CL) images were obtained. Next, LA-ICP-MS *in situ* trace element and isotope analysis were performed. Related tests and analyses were conducted at the Tianjin Institute of Geology and Mineral Resources, according to the procedures from Li *et al.* (2009). ICPMS Datacal procedures developed by Dr. Liu at the China University of Geosciences and Isoplot software developed by Kenneth R Ludwig were used for data processing, and common lead correction was handled through the Andersen (2002) method.

4.2 *Major and trace element analyses*

As part of a detailed observation of collected samples, whether in the field or under a microscope, representative samples with no weathering were crushed in a contamination-free environment to less than 200 mesh. Major elements and trace elements were analyzed at the Southwest Metallurgical Geology Laboratory, Chengdu City, Sichuan Province, China. The major elements were analysed by XRF (X-ray fluorescence spectrometer). The test methods included the weight, X-ray fluorescence, and titration methods, and the precision was better than 5%. The trace elements were analysed by the spectrometer ICE3500 atomic absorption instrument, iCAP6300, XRF, AFS2202E atomic fluorescence spectrometer, and the NexION ICP-MS 300X, 802w spectrograph. The precision was better than 5% if the trace element content was more than 10×10^{-6}; otherwise, the precision was better than 10%.

5. Results

5.1 *Zircon U–Pb geochronology*

Five representative samples were selected for the LA-ICP-MS zircon U–Pb analysis. All the results are listed in table 1 and the CL images are shown in figure 3.

Zircon grains from sample K5 are mostly light-yellow and transparent to semi-transparent. The grains occur as short column-long columnar prismatic crystals with lengths of 100∼200 μm, individually 300 μm, and length/width ratios of 1.0 to 3.0. The CL image clearly shows oscillatory zoning, suggesting a magmatic origin. The analysed zircons yield Th (48–701 ppm) and U (218–2134 ppm) with Th/U (0.11–0.65), although Th/U is relatively milder, demonstrating the magmatic origins of the grains. A total of 32 spots on 29 zircon grains are used for dating, and the edge and core gave the same age. In addition, the ages of spots 3, 9, 20, and 21 (respectively, the $^{206}Pb/^{238}U$ ages are 353, 373, 287, and 193 Ma) are younger, while the other 28 spots' $^{206}Pb/^{238}U$ ages are relatively concentrated from 405∼431 Ma. These data yield a weighted mean age of 420.6±2.6 Ma (MSWD=2.8) (figure 3a), which belongs to the Late Silurian and represents the formation age of the monzonitic granite. Moreover, because the oscillatory zoning suggests a magmatic origin, the 420.6 ± 2.6 Ma can represent the crystallisation age of the unit.

Zircon grains from sample K46-2 are mostly light-yellow and occur as short column-long columnar prismatic crystals with lengths of 100 ∼ 200 μm and an aspect ratio of 1:1 to 2:1. The CL image clearly displays oscillatory zones. Thirty-four better shaped zircon grains, which exhibit clear oscillatory zoning, were selected for dating (a total of 36 spots). Save for spots 3, 9, 20, and 21, whose ages are younger due to missing lead (respectively, the $^{206}Pb/^{238}U$ ages are 399 Ma, 348 Ma, and 397 Ma), the $^{206}Pb/^{238}U$ ages for the other 32 spots are relatively concentrated from 409∼435 Ma. These data yield a weighted mean age of 421.2 ± 1.9 Ma (MSWD=2.1) (figure 3b), belonging to the Late Silurian and representing the emplacement age of moyite.

Zircon grains from sample K13-1 are light-yellow and occur as short column-long columnar crystalline forms that are 100 ∼ 300 μm long. The CL image clearly shows oscillatory zones, suggesting a typical magmatic origin, and most of the zircons

Table 1. *LA-ICP-MS U–Pb zircon data of granites in Qimantagh area (K5, K46-2, K13-1, K21-2, K36).*

	Content ($\times10^{-6}$)				Isotope ratio						Age (Ma)					
Spots	Pb	U	Th	Th/U	$^{206}Pb/^{238}U$	1σ	$^{207}Pb/^{235}U$	1σ	$^{207}Pb/^{206}Pb$	1σ	$^{206}Pb/^{238}U$	1σ	$^{207}Pb/^{235}U$	1σ	$^{207}Pb/^{206}Pb$	1σ
K5																
1	79	1127	412	0.37	0.0671	0.0006	0.5107	0.0057	0.0552	0.0007	419	4	419	5	419	28
2	17	243	48	0.2	0.0692	0.0006	0.5369	0.0111	0.0563	0.0012	431	4	436	9	464	48
3	76	1297	435	0.34	0.0563	0.0007	0.4215	0.0045	0.0543	0.0007	353	4	357	4	382	29
4	134	2134	228	0.11	0.0658	0.0006	0.5172	0.0051	0.057	0.0006	411	4	423	4	490	25
5	23	294	85	0.29	0.0663	0.0007	0.5047	0.0134	0.0552	0.0012	414	4	415	11	421	49
6	131	1873	264	0.14	0.0654	0.0007	0.4973	0.0087	0.0551	0.0012	409	4	410	7	417	50
7	44	634	163	0.26	0.0675	0.0006	0.5252	0.0099	0.0564	0.0009	421	4	429	8	468	37
8	50	731	147	0.2	0.0682	0.0006	0.5245	0.0055	0.0557	0.0008	425	4	428	4	442	32
9	45	629	318	0.51	0.0596	0.0006	0.4519	0.0117	0.055	0.0013	373	4	379	10	412	53
10	39	535	138	0.26	0.0668	0.0006	0.5276	0.007	0.0573	0.0008	417	4	430	6	504	29
11	29	397	181	0.46	0.0672	0.0006	0.5365	0.0202	0.0579	0.0021	420	4	436	16	525	78
12	73	1083	217	0.2	0.0687	0.0006	0.5281	0.0055	0.0557	0.0007	429	4	431	4	441	30
13	30	412	149	0.36	0.0681	0.0007	0.5326	0.0081	0.0568	0.0008	424	4	434	7	482	32
14	58	837	191	0.23	0.0674	0.0006	0.5356	0.0063	0.0576	0.0009	421	4	436	5	515	33
15	81	1144	312	0.27	0.066	0.0009	0.5363	0.0155	0.0589	0.0025	412	5	436	13	565	92
16	61	863	278	0.32	0.0672	0.0007	0.5157	0.0122	0.0556	0.0011	420	4	422	10	437	45
17	56	854	194	0.23	0.0672	0.0006	0.5211	0.0048	0.0563	0.0007	419	4	426	4	463	26
18	76	1115	328	0.29	0.0671	0.0006	0.5291	0.0117	0.0572	0.0011	419	4	431	10	498	41
19	41	629	150	0.24	0.0654	0.0006	0.5085	0.0055	0.0564	0.0007	409	4	417	5	466	28
20	86	1743	701	0.4	0.0456	0.0005	0.3284	0.005	0.0523	0.0007	287	3	288	4	297	30
21	22	682	265	0.39	0.0305	0.0006	0.212	0.0088	0.0505	0.0011	193	4	195	8	217	50
22	63	970	162	0.17	0.0663	0.0006	0.506	0.0059	0.0554	0.0007	414	4	416	5	428	28
23	35	517	137	0.27	0.0649	0.0006	0.4998	0.0069	0.0559	0.001	405	4	412	6	448	39
24	64	959	178	0.19	0.0664	0.0006	0.5267	0.006	0.0575	0.0009	414	4	430	5	513	34
25	52	788	158	0.2	0.0671	0.0006	0.5107	0.005	0.0552	0.0007	419	4	419	4	421	28
26	64	946	196	0.21	0.0683	0.0006	0.5356	0.0051	0.0569	0.0007	426	4	436	4	488	29
27	67	947	229	0.24	0.0676	0.0007	0.5583	0.0055	0.0599	0.0007	421	4	450	4	601	26
28	26	337	220	0.65	0.068	0.0006	0.5418	0.0072	0.0578	0.0009	424	4	440	6	520	34
29	61	899	184	0.2	0.0684	0.0006	0.5629	0.0046	0.0597	0.0007	426	4	453	4	592	25
30	29	392	119	0.3	0.0692	0.0006	0.5299	0.0071	0.0555	0.0008	431	4	432	6	433	34
31	50	739	146	0.2	0.0682	0.0006	0.5646	0.0052	0.0601	0.0008	425	4	455	4	606	27
32	16	218	91	0.42	0.069	0.0006	0.5588	0.0112	0.0587	0.0012	430	4	451	9	556	45
K46-2																
1	44	598	182	0.3	0.0697	0.0008	0.5251	0.0077	0.0546	0.0007	435	5	429	6	396	29
2	65	970	79	0.08	0.0684	0.0006	0.5082	0.0056	0.0539	0.0005	426	4	417	5	367	23
3	44	658	203	0.31	0.0663	0.0006	0.5111	0.0059	0.0559	0.0006	414	4	419	5	449	25
4	43	625	217	0.35	0.0676	0.0005	0.5098	0.0059	0.0547	0.0006	422	3	418	5	400	25
5	56	827	206	0.25	0.0687	0.0005	0.5122	0.0056	0.0541	0.0006	428	3	420	5	375	24
6	48	700	194	0.28	0.0677	0.0005	0.5218	0.0057	0.0559	0.0006	422	3	426	5	450	24
7	61	923	199	0.22	0.0672	0.0005	0.536	0.0064	0.0579	0.0007	419	3	436	5	524	25
8	110	1178	343	0.29	0.0638	0.0006	0.5448	0.0062	0.0619	0.0007	399	3	442	5	672	25
9	56	791	399	0.5	0.0677	0.0006	0.513	0.0056	0.0549	0.0006	422	4	420	5	410	24
10	55	809	259	0.32	0.0672	0.0006	0.51	0.0061	0.055	0.0006	419	4	418	5	414	25
11	77	1146	237	0.21	0.0673	0.0005	0.5043	0.0051	0.0544	0.0005	420	3	415	4	386	22
12	33	467	129	0.28	0.0671	0.0008	0.5086	0.0073	0.055	0.0008	419	5	418	6	412	31
13	44	599	230	0.38	0.0681	0.0006	0.5298	0.0084	0.0565	0.0008	424	4	432	7	471	32
14	46	644	242	0.38	0.0675	0.0013	0.5359	0.0115	0.0576	0.0011	421	8	436	9	515	41
15	47	695	165	0.24	0.0687	0.0005	0.51	0.0058	0.0539	0.0006	428	3	418	5	365	25
16	36	469	244	0.52	0.0675	0.0007	0.5161	0.0061	0.0555	0.0006	421	4	423	5	430	25
17	69	1100	197	0.18	0.0554	0.0014	0.531	0.0066	0.0695	0.0007	348	9	433	5	915	20
18	60	885	228	0.26	0.0675	0.0006	0.5083	0.0055	0.0546	0.0006	421	4	417	5	397	23
19	36	516	185	0.36	0.0675	0.0008	0.5177	0.0065	0.0556	0.0007	421	5	424	5	436	26

Table 1. *(Continued.)*

	Content ($\times10^{-6}$)				Isotope ratio						Age (Ma)					
Spots	Pb	U	Th	Th/U	$^{206}Pb/^{238}U$	1σ	$^{207}Pb/^{235}U$	1σ	$^{207}Pb/^{206}Pb$	1σ	$^{206}Pb/^{238}U$	1σ	$^{207}Pb/^{235}U$	1σ	$^{207}Pb/^{206}Pb$	1σ
20	39	555	174	0.31	0.0692	0.0006	0.5237	0.0071	0.0549	0.0007	431	4	428	6	408	29
21	105	1188	297	0.25	0.0671	0.0006	0.5436	0.0113	0.0587	0.0006	419	4	441	9	557	22
22	75	1132	275	0.24	0.0635	0.0008	0.5291	0.006	0.0605	0.0008	397	5	431	5	620	27
23	28	398	143	0.36	0.0662	0.0006	0.5259	0.0071	0.0576	0.0008	413	3	429	6	515	29
24	53	787	176	0.22	0.0671	0.0007	0.5101	0.0052	0.0551	0.0006	419	4	418	4	418	23
25	55	839	196	0.23	0.0663	0.0007	0.5322	0.0056	0.0582	0.0006	414	4	433	5	538	23
26	38	525	226	0.43	0.0664	0.0006	0.5358	0.0093	0.0586	0.001	414	4	436	8	551	37
27	31	477	122	0.26	0.0656	0.0006	0.507	0.0065	0.0561	0.0007	409	4	416	5	456	28
28	48	694	272	0.39	0.0673	0.0006	0.5238	0.0059	0.0565	0.0006	420	3	428	5	471	24
29	59	900	197	0.22	0.0672	0.0006	0.515	0.0054	0.0556	0.0006	419	4	422	4	437	23
30	78	1062	266	0.25	0.0674	0.0005	0.5424	0.0062	0.0584	0.0006	420	3	440	5	545	23
31	88	680	185	0.27	0.0862	0.0008	2.5905	0.0569	0.2178	0.0039	533	5	1298	29	2965	29
32	56	787	266	0.34	0.0677	0.0005	0.5075	0.0063	0.0543	0.0006	422	3	417	5	385	27
33	88	1178	293	0.25	0.0697	0.0007	0.5352	0.0086	0.0557	0.0008	434	4	435	7	440	32
34	44	637	124	0.2	0.0673	0.0005	0.5138	0.0085	0.0554	0.0009	420	3	421	7	428	37
35	49	679	181	0.27	0.0678	0.0006	0.5218	0.0091	0.0558	0.0009	423	4	426	7	445	37
36	66	935	412	0.44	0.067	0.0007	0.5202	0.0055	0.0563	0.0006	418	4	425	4	465	22
K13-1																
1	19	248	141	0.57	0.0658	0.0006	0.5064	0.0046	0.0558	0.0005	411	4	416	4	444	21
2	32	482	241	0.5	0.0609	0.0006	0.4718	0.0041	0.0562	0.0005	381	4	392	3	460	20
3	2	31	10	0.32	0.0634	0.0007	0.502	0.0367	0.0574	0.0043	396	4	413	30	507	163
4	6	93	30	0.32	0.0643	0.0006	0.4905	0.0124	0.0553	0.0014	402	4	405	10	424	56
5	14	194	105	0.54	0.0645	0.0006	0.4933	0.0076	0.0554	0.0009	403	4	407	6	430	35
6	5	80	34	0.43	0.0634	0.0006	0.4963	0.0154	0.0567	0.0018	397	4	409	13	481	69
7	10	143	65	0.45	0.066	0.0006	0.5025	0.0092	0.0552	0.001	412	4	413	8	422	41
8	4	60	21	0.35	0.0651	0.0006	0.4964	0.0234	0.0553	0.0026	407	4	409	19	424	105
9	7	93	55	0.59	0.0635	0.0006	0.5038	0.0143	0.0576	0.0016	397	4	414	12	513	63
10	7	106	49	0.47	0.0635	0.0006	0.5079	0.0126	0.058	0.0014	397	4	417	10	529	54
11	9	134	58	0.43	0.0646	0.0006	0.501	0.0073	0.0563	0.0008	403	4	412	6	463	33
12	8	114	63	0.55	0.0662	0.0006	0.5115	0.0111	0.056	0.0012	413	4	419	9	454	48
13	8	110	43	0.4	0.0659	0.0006	0.5133	0.012	0.0565	0.0013	411	4	421	10	473	50
14	5	78	30	0.38	0.0644	0.0006	0.4959	0.0152	0.0558	0.0017	402	4	409	13	446	67
15	38	568	254	0.45	0.0624	0.0006	0.4701	0.0028	0.0546	0.0004	390	3	391	2	396	16
16	5	67	28	0.42	0.0659	0.0006	0.514	0.0162	0.0566	0.0018	411	4	421	13	475	70
17	9	126	75	0.6	0.0642	0.0006	0.4985	0.009	0.0563	0.001	401	4	411	7	465	40
18	10	160	68	0.43	0.0633	0.0006	0.5071	0.0103	0.0581	0.0012	396	4	417	8	534	46
19	3	50	23	0.47	0.065	0.0007	0.4982	0.0186	0.0555	0.002	406	4	410	15	434	82
20	5	65	41	0.63	0.0638	0.0006	0.5068	0.0178	0.0576	0.002	399	4	416	15	516	76
21	5	70	34	0.48	0.0634	0.0007	0.5241	0.0124	0.06	0.0014	396	4	428	10	603	50
22	29	405	243	0.6	0.0663	0.0007	0.5092	0.0044	0.0557	0.0005	414	4	418	4	439	20
23	6	98	32	0.33	0.0635	0.0006	0.521	0.0131	0.0595	0.0015	397	4	426	11	587	55
24	9	129	75	0.58	0.0644	0.0006	0.4979	0.0089	0.056	0.001	403	4	410	7	454	40
25	49	710	334	0.47	0.0646	0.0006	0.4952	0.0075	0.0556	0.0009	404	4	408	6	435	38
26	5	73	38	0.52	0.0655	0.0006	0.5157	0.0151	0.0571	0.0016	409	4	422	12	494	64
27	12	174	85	0.49	0.0625	0.0006	0.4708	0.0065	0.0546	0.0008	391	4	392	5	396	32
28	9	129	54	0.42	0.0661	0.0006	0.5191	0.0091	0.0569	0.001	413	4	425	7	490	40
29	10	175	49	0.28	0.0561	0.0007	0.4254	0.0086	0.055	0.0012	352	4	360	7	412	48
30	19	256	141	0.55	0.0672	0.0006	0.5403	0.0056	0.0583	0.0006	419	4	439	5	541	23
31	3	69	31	0.45	0.0332	0.0004	0.2319	0.019	0.0507	0.0042	211	3	212	17	225	191
32	14	200	90	0.45	0.0658	0.0006	0.5239	0.007	0.0577	0.0008	411	4	428	6	520	29

Table 1. *(Continued.)*

	Content ($\times10^{-6}$)						Isotope ratio				Age (Ma)					
Spots	Pb	U	Th	Th/U	$^{206}Pb/^{238}U$	1σ	$^{207}Pb/^{235}U$	1σ	$^{207}Pb/^{206}Pb$	1σ	$^{206}Pb/^{238}U$	1σ	$^{207}Pb/^{235}U$	1σ	$^{207}Pb/^{206}Pb$	1σ
K21-2																
1	17	257	193	0.75	0.0518	0.0005	0.3983	0.0045	0.0557	0.0008	326	3	340	4	442	32
2	14	127	199	1.57	0.0639	0.001	0.4878	0.0212	0.0554	0.0016	399	7	403	18	427	66
4	16	211	154	0.73	0.0639	0.0006	0.5023	0.0063	0.057	0.0008	400	4	413	5	490	29
5	27	374	307	0.82	0.0595	0.0006	0.4487	0.0048	0.0546	0.0008	373	4	376	4	398	32
6	38	487	861	1.77	0.0533	0.0006	0.3949	0.0066	0.0538	0.0009	334	3	338	6	362	39
7	29	390	367	0.94	0.0623	0.0006	0.4753	0.008	0.0553	0.001	390	3	395	7	425	40
8	13	181	132	0.73	0.0617	0.0005	0.4666	0.0061	0.0548	0.0007	386	3	389	5	405	30
9	15	170	224	1.32	0.0631	0.0006	0.4857	0.0058	0.0558	0.0007	395	3	402	5	445	28
10	16	191	238	1.25	0.0643	0.0006	0.4994	0.0064	0.0563	0.0008	402	4	411	5	464	30
11	16	210	192	0.91	0.061	0.0005	0.472	0.0058	0.0561	0.0007	382	3	393	5	455	28
12	23	288	297	1.03	0.0649	0.0007	0.5006	0.0051	0.056	0.0006	405	4	412	4	451	23
13	28	345	388	1.12	0.0623	0.0006	0.4878	0.0045	0.0568	0.0005	389	4	403	4	485	21
14	19	250	250	1	0.0615	0.0005	0.4926	0.0049	0.0581	0.0006	385	3	407	4	533	24
15	12	152	125	0.82	0.0641	0.0006	0.4845	0.0098	0.0548	0.001	400	4	401	8	406	42
16	25	320	302	0.95	0.0629	0.0006	0.4926	0.0042	0.0568	0.0005	393	4	407	3	485	20
17	49	542	625	1.15	0.0636	0.0007	0.4813	0.0072	0.0549	0.0006	397	4	399	6	408	26
18	21	295	200	0.68	0.0626	0.0006	0.4758	0.0061	0.0551	0.0007	391	4	395	5	417	27
19	34	450	402	0.89	0.0631	0.0006	0.4813	0.0081	0.0553	0.001	395	4	399	7	425	39
20	23	280	341	1.22	0.0634	0.0006	0.4787	0.0055	0.0548	0.0006	396	4	397	5	402	24
21	19	263	167	0.63	0.0624	0.0006	0.4693	0.0063	0.0545	0.0008	390	4	391	5	393	32
22	28	315	334	1.06	0.0652	0.0007	0.5024	0.0047	0.0559	0.0006	407	4	413	4	449	26
23	14	346	174	0.5	0.0363	0.0003	0.2759	0.0045	0.0551	0.0009	230	2	247	4	415	37
24	28	410	305	0.74	0.061	0.0005	0.4729	0.0082	0.0562	0.001	382	3	393	7	461	41
25	53	629	779	1.24	0.0638	0.0007	0.4972	0.0088	0.0565	0.0011	399	4	410	7	472	44
26	20	283	200	0.71	0.0617	0.0006	0.4686	0.0086	0.0551	0.0011	386	4	390	7	415	44
27	14	391	621	1.59	0.0249	0.0002	0.1786	0.0017	0.0519	0.0006	159	2	167	2	282	24
28	27	324	397	1.23	0.0633	0.0006	0.4937	0.0064	0.0565	0.0007	396	4	407	5	474	27
29	12	139	220	1.58	0.0607	0.0006	0.4772	0.0082	0.057	0.001	380	4	396	7	492	38
30	29	332	680	2.05	0.0599	0.0006	0.4424	0.0043	0.0535	0.0006	375	3	372	4	352	26
31	12	166	135	0.82	0.0615	0.0005	0.4706	0.0065	0.0555	0.0008	385	3	392	5	432	32
32	23	249	816	3.27	0.0608	0.0006	0.4784	0.0039	0.0571	0.0005	380	4	397	3	495	18
K36																
1	2	31	17	0.55	0.0609	0.0005	0.4923	0.0403	0.0586	0.0049	381	3	407	33	483	184
2	6	91	39	0.43	0.0618	0.0004	0.5027	0.0153	0.0589	0.0018	387	2	414	13	588	66
3	3	38	19	0.5	0.0619	0.0005	0.4886	0.0479	0.0572	0.0056	387	3	404	40	431	218
4	6	85	45	0.53	0.0605	0.0004	0.4889	0.0161	0.0586	0.0019	379	2	404	13	553	69
5	3	45	25	0.57	0.061	0.0005	0.4649	0.031	0.0553	0.0037	382	3	388	26	424	148
6	3	41	23	0.56	0.0606	0.0004	0.491	0.0301	0.0588	0.0035	379	3	406	25	727	128
7	6	85	57	0.67	0.0622	0.0004	0.4948	0.0127	0.0577	0.0015	389	2	408	10	519	55
8	5	81	34	0.42	0.0629	0.0004	0.5303	0.0147	0.0611	0.0017	393	3	432	12	644	60
9	9	136	82	0.6	0.061	0.0004	0.457	0.0157	0.0544	0.0018	382	2	382	13	386	75
10	7	111	70	0.63	0.0606	0.0004	0.4557	0.0195	0.0545	0.0023	380	3	381	16	392	94
11	6	93	40	0.42	0.061	0.0004	0.464	0.0199	0.0552	0.0023	381	2	387	17	421	94
12	7	106	68	0.64	0.0607	0.0004	0.5442	0.0129	0.065	0.0016	380	2	441	10	775	50
13	4	69	27	0.39	0.0609	0.0004	0.4796	0.0217	0.0571	0.0026	381	2	398	18	494	100
14	5	72	46	0.64	0.0603	0.0005	0.485	0.0279	0.0583	0.0033	378	3	401	23	541	123
15	6	93	49	0.53	0.0607	0.0004	0.4545	0.0136	0.0543	0.0016	380	2	380	11	384	67
16	11	165	134	0.81	0.0607	0.0004	0.4937	0.0113	0.059	0.0014	380	2	407	9	568	51
17	3	50	24	0.47	0.0606	0.0004	0.503	0.0227	0.0602	0.0027	379	3	414	19	655	97
19	5	74	31	0.42	0.0606	0.0004	0.4868	0.0163	0.0583	0.0019	379	2	403	13	750	69
20	5	75	42	0.56	0.0608	0.0004	0.5026	0.0207	0.06	0.0024	380	3	413	17	602	88
21	5	83	46	0.55	0.0608	0.0004	0.4694	0.0291	0.056	0.0034	380	3	391	24	453	135
22	5	79	37	0.46	0.0608	0.0004	0.4787	0.0144	0.0571	0.0017	380	2	397	12	496	67
23	5	80	40	0.49	0.0608	0.0004	0.4609	0.013	0.055	0.0015	380	2	385	11	413	63
24	6	92	52	0.57	0.0606	0.0004	0.4914	0.0177	0.0588	0.0021	380	2	406	15	558	77

Table 1. *(Continued.)*

	Content ($\times 10^{-6}$)						Isotope ratio				Age (Ma)					
Spots	Pb	U	Th	Th/U	$^{206}Pb/^{238}U$	1σ	$^{207}Pb/^{235}U$	1σ	$^{207}Pb/^{206}Pb$	1σ	$^{206}Pb/^{238}U$	1σ	$^{207}Pb/^{235}U$	1σ	$^{207}Pb/^{206}Pb$	1σ
25	4	71	33	0.47	0.0607	0.0004	0.4744	0.0251	0.0567	0.003	380	3	394	21	480	116
26	5	73	33	0.45	0.0607	0.0004	0.4935	0.0163	0.0589	0.0019	380	2	407	13	564	71
27	8	126	51	0.4	0.0608	0.0004	0.4726	0.0088	0.0564	0.0011	380	2	393	7	468	42
28	4	61	27	0.44	0.0608	0.0005	0.4635	0.0356	0.0553	0.0042	381	3	387	30	423	168
29	5	82	55	0.68	0.0609	0.0004	0.4586	0.0137	0.0547	0.0016	381	2	383	11	398	66
30	2	30	21	0.7	0.0607	0.0006	0.4549	0.0535	0.0543	0.0066	380	4	381	45	385	271
31	7	114	61	0.54	0.0609	0.0004	0.4561	0.0124	0.0543	0.0014	381	2	382	10	384	60
32	14	220	106	0.48	0.0604	0.0004	0.5163	0.0136	0.062	0.0017	378	2	423	11	756	58

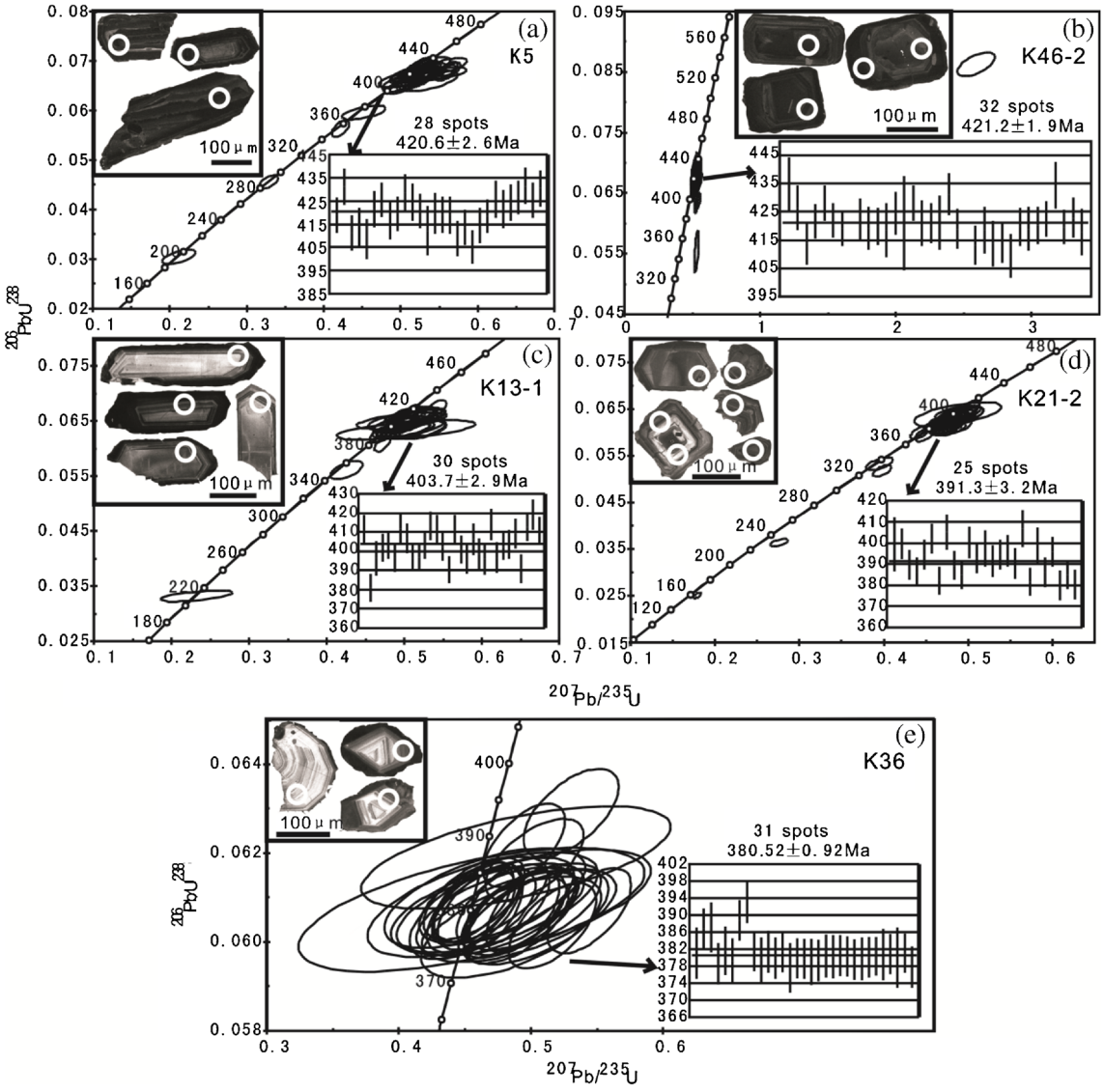

Figure 3. Cathodoluminescence (CL) images of representative zircon grains and Concordia plots of granites in Qimantage area. Solid circles indicate the locations of LA-ICP-MS U–Pb dating.

have dark hyperplasia edges. The analysed zircons have Th content and U content values of 10–334 and 31–710 ppm, respectively, with Th/U ratios from 0.28 to 0.63. Although the Th/U is relatively mild, the ratio as a whole is greater than 0.4, suggesting a magmatic origin for the zircon (Belousova *et al.* 2002; Zhong *et al.* 2006). A total of 32 spots on 28 zircon grains are used for dating, though

the ages of spots 29 and 31 (respectively, the $^{206}Pb/^{238}U$ ages are 352 and 211 Ma) are younger due to missing lead. The age of spot 29 may be the age of a late stage magmatic transformation, while the age of spot 31 may be that of late stage metamorphic or hydrothermal zircon. The other 30 $^{206}Pb/^{238}U$ ages are relatively concentrated from 381∼419 Ma. These data yield a weighted average age of 403.7 ± 2.9 Ma (MSWD =3.9) (figure 3c), which belongs to the Early Devonian and represents the formation age of granodiorite.

Zircon grains from sample K21-2 are mostly short column and much less than 100 μm, individually 100 ∼ 200 μm, and mostly show clear oscillatory zones in CL image 3, suggesting a magmatic origin. The concentrations of the trace elements Th and U in the zircon grains are larger (Th: 125–861 ppm; U: 127–629 ppm), and the change in Th/U (0.5–3.27) is relatively larger, denoting magmatic zircon as the ratios are all >0.4 (Belousova *et al.* 2002; Zhong *et al.* 2006). A total of 32 spots on 31 zircon grains are used for dating, but spot 3 has no result and spots 1, 5, 6, 23, 27, and 30 (respectively, the $^{206}Pb/^{238}U$ ages are 326, 373, 334, 230, 159, and 375 Ma) are younger. The $^{206}Pb/^{238}U$ ages of the other 25 spots are relatively concentrated from 380 to 407 Ma. These data yield a weighted average age of 391.3±3.2 Ma (MSWD= 4.3) (figure 3d), belonging to the Middle Devonian and representing the diagenetic age of granite porphyry.

Zircon grains from sample K36 are mostly light-yellow and transparent to semi-transparent, and they occur as short column prismatic crystals, though only some are long and the crystals are mostly 100 ∼ 200 μm long. The CL image shows clearly oscillatory zones, suggesting a magmatic origin. The concentrations of the trace elements Th and U in the zircon grains are 17–134 and 30–220 ppm, respectively. The change in Th/U (0.39–0.81) is relatively milder, though almost all the ratios are >0.4, showing magmatic zircon (Belousova *et al.* 2002; Zhong *et al.* 2006). Because of the numerous zircon grains in this sample, we only selected 31 of them (a total of 32 spots) for dating. Spot 18 has no result, while the $^{206}Pb/^{238}U$ ages of the other 31 spots are relatively concentrated from 378 to 393 Ma. These data yield a weighted mean age of 380.52 ± 0.92 Ma with a small MSWD value (0.62) (figure 3e), belonging to Late Devonian and representing the formation age of granodiorite.

5.2 *Whole rock geochemistry*

The major and trace element analysis results of the Late Silurian–Late Devonian granitoids in the Qimantagh area are listed in table 2.

5.2.1 *Major elements*

The Late Silurian granitoid belongs to the subalkaline series (figure 4a), consisting mainly of monzonitic granite and rarely granodiorite and alkali-granite (figure 4b). Overall, the rock types plot in the high-K calc-alkaline field in the K_2O *vs.* SiO_2 diagram (figure 4c). They exhibit metaluminous to weakly and strongly peraluminous characteristics on a plot of A/NK *vs.* A/CNK (figure 4d).

The Early Devonian granitoid also belongs to the subalkaline series (figure 4a), but the lithology is relatively scattered, including quartz diorite, quartz monzodiorite, and especially granodiorite and monzogranite (figure 4b). In the K_2O *vs.* SiO_2 diagram (figure 4c), the rock types mainly plot in the high-K calc-alkaline field in general. All the same, they also exhibit metaluminous to weakly and strongly peraluminous characteristics on a plot of A/NK *vs.* A/CNK (figure 4d).

The Middle Devonian granitoid belongs to the subalkaline series, but it has a trend towards an alkaline series evolution (figure 4a). The lithology of the Middle Devonian granitoid is mainly monzonitic granite and granodiorite (figure 4b), but at the same time, this stage shows high potassium characteristics. The rock types mainly plot in the high-K calc-alkaline field, though parts of them drop into the shoshonite field (figure 4c). In the A/NK *vs.* A/CNK diagram, they exhibit metaluminous to weakly peraluminous characteristics (figure 4d).

The Late Devonian granitoid also belongs to the subalkaline series (figure 4a), but the lithology is relatively scattered, including quartz diorite, quartz monzodiorite, and especially granodiorite and monzonitic granite (figure 4b). The rock types mainly plot in the high-K calc-alkaline field, though parts of them distributed into the medium-K calc-alkaline field in the K_2O *vs.* SiO_2 diagram (figure 4c). As with the Late Silurian and Early Devonian granitoids, the Late Devonian granitoid exhibits metaluminous to weakly and strongly peraluminous characteristics on a plot of A/NK *vs.* A/CNK (figure 4d).

5.2.2 *Trace elements*

The Late Silurian granitoid has chondrite-normalised REE patterns (figure 5a) that are enriched in light rare earth elements (LREE) (LREE/HREE=4.76–18.15, average 9.08 $(La/Yb)_N = 4.33$–33.36, average 11.91), with moderately negative Eu anomalies (0.15–0.86, average 0.53), and are depleted in heavy rare earth elements (HREE) ($(Tb/Yb)_N$ =1.06–2.5, average 1.51).

Table 2. *The major and trace element analysis results of Late Silurian–Late Devonian granitoids in Qimantageh area.*

Sample no	4013	4020-1	3019b	7018	2009-1	6024-1	P72-1	IIP21Gs4-1	IIGs4589	IIP21Gs2-1	IIGs3238-1	6PM202GS17-1	6GS2986	6GS2988
Source	Bai *et al.* (2004)							Wang (2011)				Tan *et al.* (2011)		
Age	Late Silurian													
SiO_2	66.71	73.61	75.85	71.25	71.26	65.25	76.1	68.59	72.95	66.94	69.88	70.47	72.33	72.84
TiO_2	0.85	0.33	0.14	0.45	0.39	0.88	0.1	0.59	0.31	0.75	0.43	0.34	0.14	0.32
Al_2O_3	14.02	13.02	12.31	12.85	13.62	14.74	11.75	14.64	13.53	14.67	13.69	13.7	14.47	14.07
Fe_2O_3	2.12	1.71	1.17	1.51	1.41	2.36	1.17	0.45	0.32	0.73	0.85	0.26	0.07	0.37
FeO	2.93	1.52	0.81	1.17	1.14	2.79	0.7	3.57	2.03	4.55	3.27	3.03	1.48	1.17
MnO	0.18	0.03	0.02	0.04	0.04	0.07	0.02	0.08	0.08	0.11	0.09	0.07	0.03	0.02
MgO	1.19	1.24	0.28	0.09	1.06	1.19	0.14	1.09	0.7	1.66	0.75	1.06	0.51	0.9
CaO	2.88	0.15	0.83	2.75	2.11	4.79	1.15	2.4	1.01	2.41	1.75	1.81	1.74	1
Na_2O	3.16	3.96	3.76	3.08	4.46	3.06	3.68	2.31	2.72	1.99	2.99	2.92	3.06	3.27
K_2O	3.56	2.72	3.92	5.08	3.42	3.36	4.7	4.17	4.7	3.69	4.49	3.97	4.75	4.59
P_2O_5	0.15	0.06	0.02	0.1	0.09	0.18	0.01	0.09	0.07	0.12	0.09	0.06	0.07	0.07
H_2O^+	1.04	0.62	0.18	0.28	0.82	0.64	0.16	1.75	1.28	2.06	1.37	1.49	0.8	1.08
								0.06	0.15	0.08	0.14			
LOS	0.87	0.33	0.33	0.75	0.57	0.57	0.32					0.6	0.14	0.14
La	23.68	80.4	40.46	62.98	29.16	57.28		39.51	26.8	41.57	47.75	37.93	44.65	45.45
Ce	56.12	172.7	89.34	133.6	52.38	113.3		75.14	52.14	79.34	94.33	72.62	82.49	83.55
Pr	6.95	19.33	10.4	13.74	6.02	12.51		9.55	6.89	9.83	10.69	8.15	9.29	9.22
Nd	28.55	68.25	38.09	45.65	19.52	44.71		35.73	23.98	36.34	42.2	27.41	32.99	33.3
Sm	7.05	13.77	8.85	8.1	3.23	8.1		7.47	5.41	7.4	8.76	5.17	5.6	5.89
Eu	1.34	0.66	0.47	1.15	0.81	1.63		1.23	0.71	1.29	1.4	1.11	1.05	1.04
Gd	7.4	13.05	8.78	6.99	2.3	7.23		6.64	4.94	6.4	8.3	4.87	4.02	4.17
Tb	1.252	2.25	1.636	1.197	0.319	1.146		1.08	0.91	1.08	1.3	0.77	0.52	0.55
Dy	7.24	13.13	10.07	6.66	1.54	6.3		5.99	5.42	6.32	7.36	4.27	2.41	2.55
Ho	1.41	2.61	2.19	1.42	0.28	1.32		1.22	1.15	1.4	1.54	0.92	0.46	0.48
Er	3.89	4.18	6.32	3.98	0.75	3.76		3.24	3.12	3.9	4.39	2.58	1.03	1.09
Tm	0.595	1.096	1.054	0.65	0.124	0.599		0.51	0.5	0.64	0.68	0.42	0.16	0.18
Yb	3.69	6.64	6.7	3.93	0.71	3.75		3.04	3.15	3.89	4.21	2.8	0.96	1
Lu	0.512	0.921	0.989	0.59	0.105	0.567		0.48	0.49	0.61	0.67	0.44	0.14	0.15
Y	36.93	70.96	57.52	37.1	7.97	34.95		27.93	28.3	33.26	39.06	24.7	11.33	12.01
Ba	722	258		548		1057	65.4	614	378	742	769	965	840	675
Rb	159	150		201		91.5	257	192	243	179	163	169	200	190
Th	12.9	24.5		27.3		12	35.9	15.4	15.2	14.9	20.7	13	22.6	20.7
Nb	0	0		0		1.1	0	13.7	11.7	15.7	16.9	10.2	12	10.9
Ta	0	0.94		1.4		2.1	2.9	1.4	2	1.4	1.3	1.07	1.73	1.17
Sr	161	84		115		69.5	23.4	123	75.4	227	156	164	281	193
Zr	384	289		392		533	130	161	126	180	228	153	156	161
Hf	10	7.7		10.1		14.1	5.2	5.4	4.4	5.9	6.4	4.9	6.2	5.9

Table 2. *(Continued.)*

Sample no.	6PM202GS6-1	6PM202GS7-1	6PM202GS9-1	6PM202GS11-1	K5	K46-2	5094	IP31GS2-1	I74GS5060	IP31→GS3-5	186GS5143-1	IIP31Dy7-1	IIGs3209-1
Source	Tan *et al.* (2011)				This paper		Bai *et al.* (2004)	Wang (2011)					Wang *et al.* (2004)
Age	Late Silurian						Early Devonian						
SiO_2	71.36	71.98	72.17	69.91	68.77	65.13	70.37	65.05	71.26	71.33	72.07	75.51	60.71
TiO_2	0.3	0.3	0.29	0.31	0.43	0.52	0.36	0.9	0.48	0.22	0.15	0.08	1.19
Al_2O_3	14.02	13.45	13.45	13.79	14.52	15.39	13.43	14.67	13.52	14.1	14.23	13.36	15.82
Fe_2O_3	0.62	0.38	0.9	0.61	0.32	0.84	1.48	1.09	0.93	1.65	1.67	0.19	1.74
FeO	2.23	2.27	1.93	3.17	3.27	3.74	2.6	5.68	2.88	0.05	0.84	0.97	5.82
MnO	0.05	0.04	0.05	0.05	0.068	0.089	0.07	0.12	0.073	0.5	0.04	0.13	0.13
MgO	0.65	1.85	0.71	1.91	1.06	2.71	0.78	2.11	1.41	0.93	0.46	0.25	1.63
CaO	2.77	0.73	1.82	0.66	2.61	1.89	1.58	2.16	2.06	2.86	0.84	1.67	4.06
Na_2O	2.9	3.1	2.71	3.9	3.23	2.87	2.93	1.99	3.66	5.45	3.07	2.4	3.49
K_2O	3.67	3.76	4.16	2.92	4.29	4.60	4.64	3.87	2.1	0.2	5.06	4.02	3.83
P_2O_5	0.04	0.05	0.05	0.05	0.11	0.12	0.16	0.17	0.12	0.83	0.16	0.04	0.36
H_2O^+	1.09	1.7	1.28	1.85			1.11	1.47	0.48		0.78	0.86	0.51
								2.22	1.05		0.91	0.27	
LOS	0.12	0.22	0.28	0.7	0.91	1.94	0.67						0.48
La	34.41	33.21	42.47	18.12	32.41	49.12	37.64	39.55	27.91	27.25	19.95	48.27	18.47
Ce	63.54	61.13	80.44	34.6	70.54	78.10	83.53	87.26	61.37	54.72	36.11	95.36	38.56
Pr	7.12	6.99	8.77	3.77	7.71	9.43	10.44	12.72	7.6	7.01	4.12	11.56	4.67
Nd	27.1	25.89	34.17	14.52	31.869	36.93	37.23	50.01	26.23	24.95	17.209	42.34	15.66
Sm	5.22	4.74	6.73	3.17	5.52	7.04	8.62	11.77	5.97	5.46	2.92	7.95	3.1
Eu	1.04	0.86	1.2	0.65	1.08	1.32	0.94	3.11	1.14	1.43	0.81	1.37	0.72
Gd	5.22	4.61	6.95	3.78	5.56	7.37	7.52	10.2	6.12	4.84	3.08	7.33	2.74
Tb	0.84	0.71	1.15	0.58	0.82	1.14	1.24	1.77	0.96	0.76	0.44	1.13	0.46
Dy	4.97	3.86	6.81	3.52	4.45	6.21	6.89	10.02	5.84	4.23	2.37	6.21	2.51
Ho	1.08	0.79	1.46	0.76	0.92	1.22	1.42	1.94	1.16	0.83	0.50	1.31	0.48
Er	3.13	2.22	4.23	2.24	2.44	3.47	4.02	4.94	3.3	2.04	1.43	3.58	1.34
Tm	0.53	0.36	0.67	0.37	0.37	0.48	0.58	0.68	0.52	0.28	0.20	0.55	0.21
Yb	3.39	2.4	4.2	2.48	2.819	2.96	3.87	4.18	3.32	1.69	1.32	3.43	1.24
Lu	0.53	0.38	0.63	0.42	0.32	0.41	0.54	0.59	0.5	0.23	0.22	0.5	0.19
Y	28.65	20.96	37.84	21.87	27.31	34.09	37.08	42.79	32.96	19.94	14.25	32.9	13.74
Ba	626	661	716	486	582.9	684.1	343	1550	580	865	603.2	276	770
Rb	121	127	131	92.6	204.63	223.34	267	144	195	152.8	93.56	295	144
Th	15.1	15.7	17.2	16	20.454	22.192	32.9	7.1	14.7	18.6	7.565	14.3	13
Nb	10.3	8.87	10.2	9.69	16.52	23.69	17.2	24.5	14.7	14.2	7.24	11.1	16.9
Ta	1.03	0.94	0.99	0.92	2.593	3.354	2.3	1.6	0.5	1.1	0.804	0.9	1.7
Sr	138	84.9	135	70.2	251.3	165.6	87	298	148	164	312.5	80	159
Zr	150	156	173	173	175.35	207.72	245	644	281	219	114.39	101	112
Hf	4.4	4.6	5	4.3	9.95	8.669	7.1	12.4	7.1	5	5.856	3.6	4.6

Table 2. *(Continued.)*

Sample no.	IIGs5215-1	IIGs6103-1	K13-1	I86GS5009-1	4032[a]	6PM102Gs2-1	6PM102GS5-1	6PM102GS8-1	Gs5116-1	6PM403GS2-1	6PM403GS2-2	6PM403GS3-1	6PM403GS4-1
Source	Wang *et al.* (2004)		This paper	Wang (2011)		Wang (2011)							
Age	Early Devonian					Middle Devonian							
SiO_2	67.98	67.96	68.56	58.68	57.99	71.14	71.89	71.26	73.25	69.44	69.05	69.91	69.62
TiO_2	0.76	0.54	0.33	0.82	1.09	0.4	0.39	0.47	0.25	0.74	0.57	0.69	0.76
Al_2O_3	13.56	14.32	14.85	17.04	16.21	13.66	13.68	13.91	12.61	12.87	14.43	13.57	13.15
Fe_2O_3	2.22	0.88	0.74	2.96	4.3	0.24	0.27	0.53	1.46	0.29	0.32	0.44	0.48
FeO	2.73	2.98	3.63	3.34	4.51	2.38	1.78	2.13	1.6	3.72	3.15	3.47	3.68
MnO	0.084	0.05	0.05	0.08	0.2	0.04	0.03	0.04	0.05	0.06	0.05	0.06	0.07
MgO	1.64	1.52	1.22	3.33	2.11	0.72	0.57	0.6	0.4	0.95	0.92	0.99	0.94
CaO	2.82	2.64	3.13	3.13	4.15	1.5	1.46	1.37	1.15	2.77	2.11	2.94	1.91
Na_2O	2.62	2.69	3.86	6.04	3.4	3.29	3.13	3.17	2.72	2.36	2.62	2.94	2.47
K_2O	4.26	3.73	2.83	1.01	2.76	4.32	5.07	5.03	5.35	4.01	5.21	2.95	4.7
P_2O_5	0.26	0.24	0.067	0.16	0.21	0.13	0.08	0.1	0.06	0.17	0.15	0.16	0.19
H_2O^+	1.17	0.72		2	1.62	1.19	0.97	1.11	0.79	1.4	1.05	1.13	1.33
LOS	1.25	2.12	0.33	1.1	0.84	0.85	0.5	0.12	0.19	1.02	0.16	0.59	0.49
La	19.73		19.93	43.77	27.7	43.66	29.15	69.86	58.53	70.22	51.76	100.8	49.27
Ce	40.23		36.05	96.18	57.79	86.45	52.91	135.1	121.6	138.9	103.9	189.5	101.8
Pr	5.27		4.01	11.22	6.57	10.03	6.2	15.52	17.74	15.4	12.22	21.18	11.54
Nd	18.24		14.69	38.8	23.69	37.73	22.96	55.44	44.88	53.81	43.76	70.66	41.06
Sm	4.26		2.76	7.12	4.98	7.81	4.61	10.49	9.5	9.7	8.61	11.51	7.92
Eu	0.8		0.71	1.56	1.74	0.83	1.01	0.94	0.6	1.29	1.25	1.53	1.48
Gd	3.49		2.63	5.42	4.76	7.53	4.57	9.63	7.88	8.25	7.92	9.27	7.46
Tb	0.46		0.44	0.87	0.8	1.09	0.68	1.42	1.28	1.21	1.14	1.32	1.06
Dy	2.08		3.16	4.35	4.53	5.98	3.88	7.68	6.58	6.15	6.42	7.02	5.36
Ho	0.34		0.76	0.84	0.98	1.23	0.84	1.59	1.32	1.22	1.29	1.4	1.08
Er	0.84		2.68	2.11	2.8	3.4	2.29	4.11	4.24	3.08	3.42	3.57	2.77
Tm	0.12		0.46	0.32	0.46	0.54	0.38	0.63	0.61	0.44	0.49	0.49	0.41
Yb	0.72		3.08	1.9	2.89	3.4	2.5	3.81	4.14	2.53	2.96	2.85	2.46
Lu	0.1		0.43	0.28	0.44	0.53	0.38	0.57	0.61	0.38	0.44	0.43	0.38
Y	9.76		21.26	23.04	25.43	33.59	22.93	39.48	37.7	30.11	33.14	33.52	27.55
Ba	821	639	881.2	140	334	411	608.4	453.6	249	590	664	272	682
Rb	249	90	99.4	31.4	65.6	233	187.5	199.7	317	183	225	209	222
Th	25.6	23.1	5.6	23.1	9.8	24.5	11.2	28.3	57.1	28.3	23.5	16.8	31.1
Nb	4.9	12.1	10.5	0	0	17.2	13.1	17.6	9.7	24.2	18.3	19.6	31.6
Ta	<0.5	0.6	0.6	2	1.7	1.8	1.9	1.7	0.7	2	1.1	0.9	1.6
Sr	64	107	215.7	80.1	189	117	165.7	101.3	87	189	199	196	194
Zr	252	361	85.5	299	353	187	184.2	235.1	193	244	215	225	292
Hf	7.9	8	2.9	8.3	9	6.7	6.9	7.5	5.8	7.3	7.2	7.3	9.1

Table 2. *(Continued.)*

Sample no.	6PM403GS4-2	6PM403GS4-3	6GS1144-1	6GS1395-1	6GS1583	6GS1213	6GS1923	6PM103Gs4-1	6PM103Gs5-1	6PM103Gs7-1	6PM103Gs8-2	K21-2	5058
Source	Wang (2011)							Guo *et al.* (2011)				This paper	Bai *et al.* (2004)
Age	Middle Devonian												
SiO_2	66.58	68.91	64.15	67.93	70.8	74.97	72.2	76.73	74.41	76.92	76.17	74.30	75.09
TiO_2	0.81	0.71	0.89	0.69	0.65	0.22	0.16	0.12	0.25	0.1	0.12	0.23	0.21
Al_2O_3	14.7	13.94	14.81	14.86	13.57	12.28	13.85	12.17	12.81	12.17	12.57	11.94	13.48
Fe_2O_3	0.37	0.34	0.77	0.22	0.16	0.51	0.01	0.23	0.32	0.18	0.18	1.58	0.74
FeO	4	3.45	4.28	3.65	3.3	1.22	0.98	0.62	1.22	0.75	0.7	1.71	1.24
MnO	0.07	0.06	0.08	0.06	0.04	0.04	0.02	0.02	0.04	0.03	0.03	0.039	0.03
MgO	1.2	1.06	1.39	1.02	0.91	0.4	0.2	0.14	0.39	0.1	0.15	0.72	0.16
CaO	2.58	2	3.4	3.16	3.1	1.14	0.87	0.7	1.35	0.56	0.58	1.05	1.29
Na_2O	2.76	2.82	2.99	3.28	3.18	2.78	2.65	3.23	3.29	3.5	3.04	1.87	3.42
K_2O	4.73	4.8	4.49	3.62	2.77	5.17	7.79	5.08	4.92	4.96	5.56	5.37	3.88
P_2O_5	0.17	0.15	0.21	0.16	0.15	0.04	0.03	0.01	0.05	0.01	0.01	0.031	0.05
H_2O^+	1.33	1.17	1.29	1.02	0.84	0.79	0.45	0.57	0.62	0.46	0.61		0.4
						0.17	0.7	0.26	0.2	0.15	0.15		
LOS	0.49	0.38	1	0.12	0.32							0.91	0.42
La	77.39	45.72	28.61	23.99	35.92	133	72.2	17.48	33.52	20.24	38.73	44.38	29.68
Ce	147.9	89.85	59.22	47.14	71.9	242	141.4	41.66	66.69	50.02	80.92	64.28	59.9
Pr	15.94	10.44	7.17	5.59	8.53	26.3	15.04	4.83	8.07	5.78	8.98	7.41	6.82
Nd	55.28	41.1	28.05	24.27	34.64	96.5	54.76	17.33	28.36	21.43	31.36	25.113	23.78
Sm	9.39	8.26	5.97	5.61	7.27	14.8	10.73	4.31	6.15	5.65	6.21	4.86	5.2
Eu	1.28	1.72	1.59	1.31	1.28	0.63	1.62	0.21	0.49	0.16	0.32	0.68	0.81
Gd	8.06	7.69	5.85	5.49	6.82	9.58	9.57	4.79	6.1	5.89	5.53	4.83	5.3
Tb	1.11	1.18	0.86	0.88	1.08	1.18	1.45	0.85	1.08	1.07	0.93	0.70	0.99
Dy	6.02	6.16	4.67	4.85	5.83	5.96	7.74	5.67	6.72	7.04	5.43	3.89	5.96
Ho	1.24	1.27	1	0.98	1.23	1.09	1.54	1.26	1.38	1.6	1.15	0.84	1.06
Er	3.2	3.4	2.6	2.63	3.32	3.24	3.74	4.15	4.24	5.19	3.52	2.63	2.96
Tm	0.5	0.52	0.41	0.41	0.53	0.44	0.53	0.67	0.63	0.89	0.52	0.41	0.42
Yb	3.1	3.12	2.48	2.53	3.26	2.91	2.78	4.61	4	6.3	3.29	2.87	2.43
Lu	0.48	0.5	0.39	0.39	0.5	0.43	0.36	0.76	0.63	0.96	0.5	0.47	0.32
Y	31.32	35.22	25.7	24.55	31.78	31.4	10.3	38.58	38.59	46.4	31.86	27.84	33.84
Ba	762	688	952	723	508	183	536	72	166	25	104	234	770
Rb	226	224	132	117	97	267	280	380	294	425	268	235.74	144
Th	19.9	26	10.8	7	7	54.2	15.5	39.8	35.2	46.1	33.4	38.011	13
Nb	22.8	19.5	18.9	15.8	17.5	96.5	13.68	17.33	15.4	14	11.3	16.61	16.9
Ta	1.7	1.4	1.2	1.1	1.5	1.41	1.81	2.2	2.4	2.73	1.54	1.69	1.7
Sr	240	197	227	214	191	83.1	79.4	36.8	56.5	18.7	38.1	78.53	159
Zr	255	239	289	249	247	256	63	106	135	98	101	145.77	112
Hf	8.3	7.7	8.2	7.6	7	7.3	2	3.8	4.3	3.8	3.5	13.127	4.6

Table 2. *(Continued.)*

Sample no.	4032-1	48-1	35-1	5020	K36	IIGs2102	IIP11Gs6-1	IIP11Gs5-1	IIP6Gs1-4	IIGs3216-1	IIP30Gs4-1	IIP11Gs4-1	IIP30Gs1-1	IIP30Gs2-1	IIP30Gs5-1
Source	Bai *et al.* (2004)				This paper	Wang (2011)									
Age	Late Devonian														
SiO_2	70.34	68.45	57.18	56.03	66.95	70.47	72.42	71.87	72.88	70.18	65.52	67.34	64.42	64.9	66.15
TiO_2	0.46	0.54	1.5	1.16	0.53	0.46	0.25	0.28	0.17	0.45	0.58	0.66	0.55	0.53	0.52
Al_2O_3	13.19	14.38	16.02	15.05	14.44	14.11	14.07	14.4	14.02	14.57	14.9	14.78	14.98	15.05	14.6
Fe_2O_3	2.66	1.18	2.24	4.22	1.74	2.36	0.93	0.93	0.18	0.78	1.04	1.05	0.34	1.48	1.24
FeO	1.98	2.72	5.08	4.69	3.45	0.97	1.00	0.85	1.13	1.1	2.3	3.75	1.45	2.65	2.07
MnO	0.09	0.08	0.12	0.14	0.11	0.05	0.04	0.01	0.02	0.03	0.07	0.04	0.05	0.06	0.05
MgO	0.32	1.42	4.63	4.04	1.08	0.81	0.44	0.41	0.41	0.58	2.3	1.15	1.11	2.31	2.08
CaO	2.62	1.72	5.21	9.07	2.33	2.13	1.38	1.11	1.6	1.2	2.66	1.73	4.18	2.09	2.28
Na_2O	2.68	2.78	3.06	1.68	4.14	3.44	3.94	4.53	2.67	4.8	4.61	4.88	6.17	5.06	4.87
K_2O	3.68	3.68	2.2	1.1	3.14	4.03	4.14	4.2	5.72	4.28	2.96	2.63	2.04	2.71	2.6
P_2O_5	0.1	0.14	0.53	0.22	0.12	0.09	0.08	0.09	0.09	0.16	0.19	0.13	0.19	0.17	0.17
H_2O^+	1.16	0.97	1.42	1.82		0.78	0.85	0.84	0.64	0.99	1.78	1.44	1.22	1.82	1.7
LOS	0.04	1.33	1.04	0.96	1.74	0.09	0.19	0.23	0.16	0.69	0.82	0.19	3.08	0.92	1.45
La	52.86	28.66		29.33	32.71		39.79	40.72	36.29	43.66	40.46	32.31	11.55	26.76	80.31
Ce	108.6	55.73		65.93	57.16		68.68	66.59	69.16	85.59	89.34	57	27.78	54.43	155.4
Pr	11.89	7.17		7.76	7.25		8.12	7.68	8.59	10.18	10.4	6.67	4.09	6.28	17.65
Nd	41.58	25.36		29	34.873		25.16	27.68	31.88	38.28	38.09	23.76	16.12	22.36	61.9
Sm	8.09	5.06		6.15	6.09		3.81	4.45	5.24	6.23	8.85	4.03	4.22	4.49	11.56
Eu	1.23	0.96		1.24	1.48		1	1.16	1.49	1.6	0.47	1.2	1.33	1.2	1.35
Gd	7.25	4.36		5.5	6.59		2.88	3.42	4.06	4.5	8.78	3.1	4.79	4.18	10.09
Tb	1.202	0.74		0.91	1.01		0.4	0.49	0.58	0.6	1.64	0.42	0.84	0.68	1.49
Dy	6.95	4.07		4.97	5.62		2.09	2.55	2.78	2.97	10.07	2.02	5.04	3.66	7.83
Ho	1.47	0.8		1.02	1.25		0.45	0.53	0.53	0.56	2.19	0.39	1.16	0.7	1.57
Er	3.95	2.34		2.91	3.48		1.23	1.4	1.24	1.37	6.32	1	3.19	2.15	4.06
Tm	0.628	0.36		0.48	0.49		0.19	0.22	0.19	0.2	1.05	0.16	0.5	0.34	0.61
Yb	3.86	2.34		2.91	3.21		1.08	1.41	1.1	1.23	6.7	1.01	2.87	2.06	3.48
Lu	0.564	0.32		0.44	0.49		0.17	0.21	0.17	0.18	0.99	0.17	0.48	0.31	0.52
Y	36.93	24.9		26.65	31.97		11.43	12.65	12.24	13.25	57.52	9.12	27.29	21.01	38.49
Ba	697	490	736	522	496.6	779	1121	1013	1747	731	758	1039	495	859	473
Rb	697	162	106	67.8	129.87	127	150	127	136	117	93	57.2	58.5	78.7	79.9
Th	23	11.6	5.4	12.5	11.185	23.6	20.4	10.4	25	22.1	14	6.1	12.2	10	13
Nb	14	14.1	0.5	14.32	13	16.2	9.4	6	7.6	8.7	15.4	6.5	7.8	6.3	
Ta	1.2	1.7	1.8	20.1	1.35	1.1	1.5	1	0.6	0.7	0.6	1.1	0.5	0.6	0.4
Sr	134	107	894	243	218.4	136	430	364	280	100	429	133	262	320	245
Zr	269	123	78.6	173	251.83	269	154	150	115	168	182	412	172	176	166
Hf	7.8	4	3.2	5.3	7.906	7.4	5.4	5.2	3.8	5.1	5.2	10.3	4.6	4.6	4.6

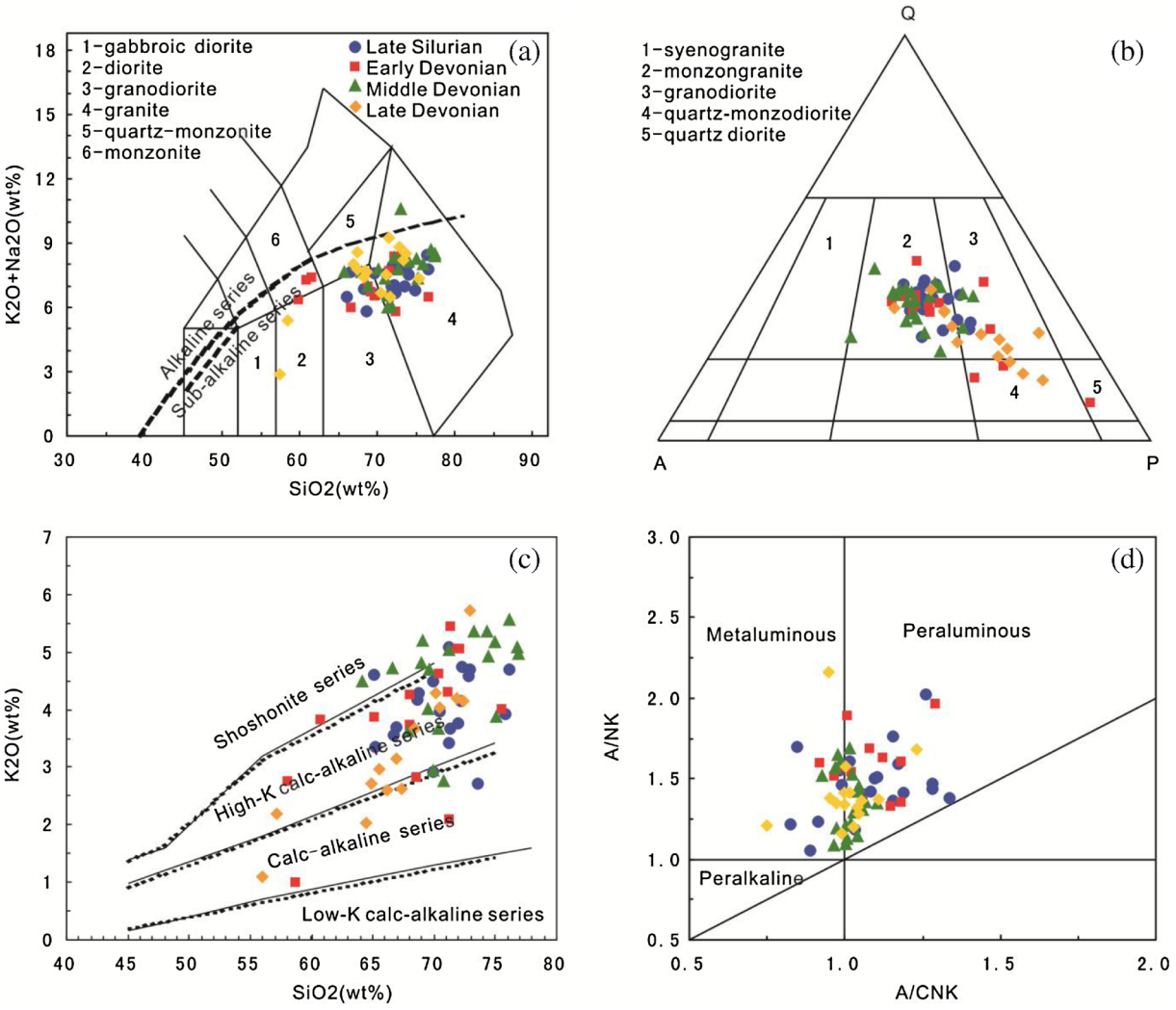

Figure 4. **(a)** (Na_2O+K_2O) *vs.* SiO_2 plot; **(b)** Quartz-alkali-feldspar diagram; **(c)** K_2O *vs.* SiO_2 plot; **(d)** A/NK *vs.* A/CNK plot. Symbols: solid line according to Peccerillo and Taylor (1976) and short dash line according to Middlemost (1985).

The Early Devonian granitoid has chondrite-normalised REE patterns (figure 5b) that are also enriched in LREE (LREE/HREE=5.73–12.35, average 8.07 $(La/Yb)_N$ =4.64–19.66, average 10.06), with weakly negative Eu anomalies (0.35–1.08, average 0.72) that occasionally trend towards positive anomalies, and border on flat HREE ($(Tb/Yb)_N$= 0.65–2.90, average 1.67) on the whole, though some may be slightly enriched in HREE.

The Middle Devonian granitoid has chondrite-normalised REE patterns (figure 5c) that are also enriched in LREE (LREE/HREE=3.57–20.67, average 9.40 $(La/Yb)_N$=2.30–32.78, average 12.75), with somewhat strongly negative Eu anomalies (0.08–0.81, average 0.40), and are depleted in HREE ($(Tb/Yb)_N$=0.77–2.37, average 1.58), though some may be slightly enriched in HREE.

The Late Devonian granitoid has chondrite-normalised REE patterns (figure 5d) that are greatly enriched in LREE (LREE/HREE=6.30–29.09, average 13.20 $(La/Yb)_N$=7.23–53.96, average 19.97), with weakly negative Eu anomalies (0.47–1.18, average 0.82) that trend towards strongly negative, and as a whole have nearly flat HREE ($(Tb/Yb)_N$=1.42–2.40, average 1.79). In addition, the Late Devonian granitoid shows similar characteristics to the Early Devonian granitoid, which may reflect the similarity of their source rock and tectonic environment.

In the primitive-mantle normalised spidergrams (figure 6), the Late Silurian–Late Devonian granitoid shows similar or roughly consistent trace element characteristics; namely, they are enriched in large ion lithophile elements (LILE), such as Rb, Th and K, and high field strength elements (HFSE), such as Zr and Hf, and are depleted in Ba, Nb, Ta, Sr, P, Eu, and Ti. The enrichment and depletion of trace elements in the Late Silurian–Late Devonian granitoid may be slightly

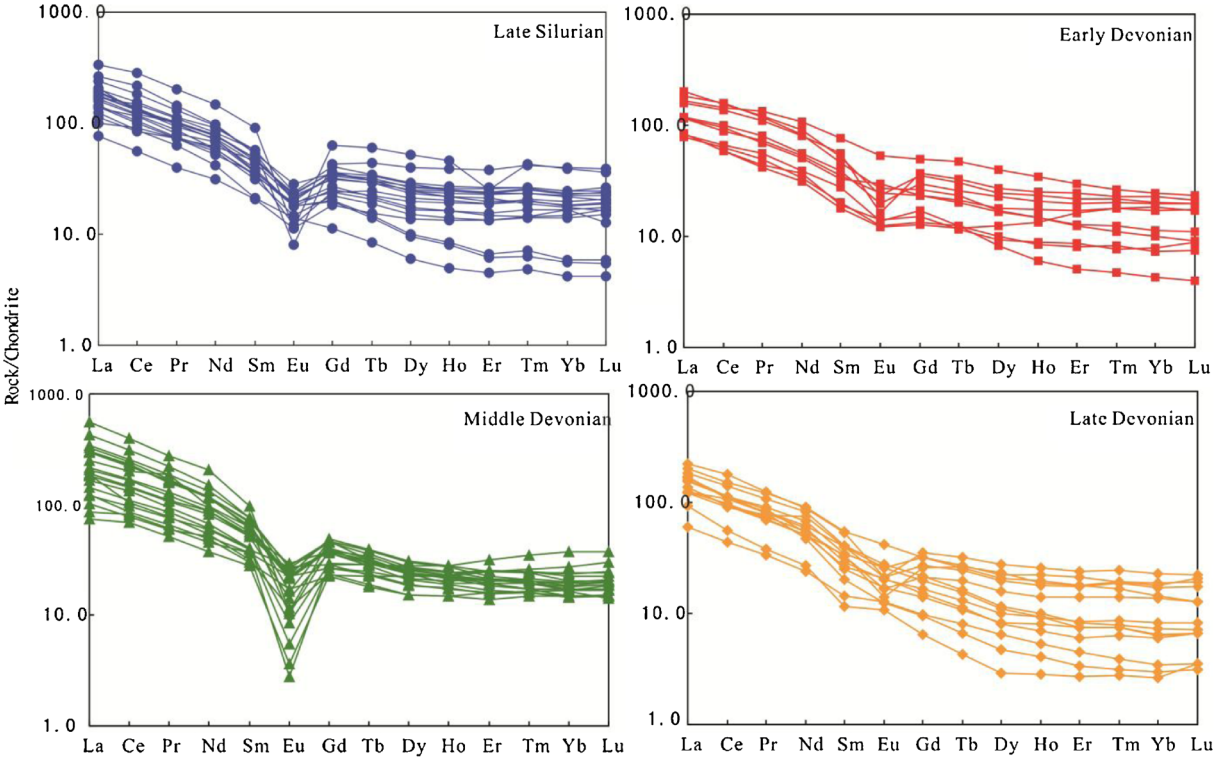

Figure 5. Chondrite-normalized REE patterns (after Sun and McDonough 1989). Symbols as in figure 4(a).

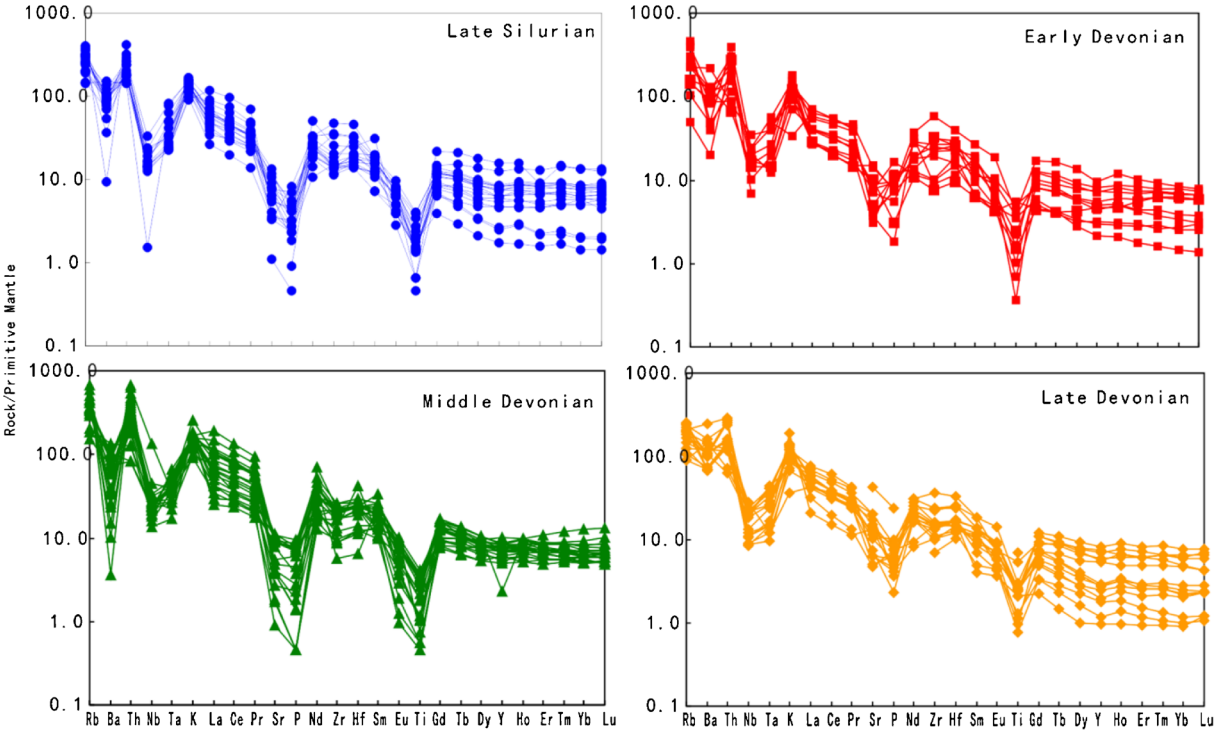

Figure 6. Primative mantle-normalized trace element spidergrams (after Sun and McDonough 1989). Symbols as in figure 4(a).

different over time, which may be related to the main and accessory minerals in the rock and the specific environment. However, these trace element characteristics are still very similar to those of volcanic arc granites in a subduction environment.

6. Discussion

6.1 *Timing of multiperiodic magmatism in the Late Silurian to Late Devonian*

According to the LA-ICP-MS zircon U–Pb dating results, multiperiodic magmatic activity existed in the Qimantagh area during the Late Silurian (approximately 420 Ma)–Late Devonian (approximately 380 Ma). In addition, the majority of $^{206}Pb/^{238}U$ ages of the zircon grains are small values, mainly in the two periods 399–373 and 353–326 Ma (respectively, Middle–Late Devonian and Early Carboniferous), which suggests that there was significant magmatic activity that made some zircon grains recrystallise. K21-2 and K36 (391.3 and 380.52 Ma recrystallisation ages, respectively) also confirmed that Middle–Late Devonian magmatic activity existed in the study area. Early Carboniferous (353–326 Ma) magmatic activity may be associated with the opening of the south Kunlun ocean basin. In addition, there are smaller $^{206}Pb/^{238}U$ ages matching the Early Permian (287 Ma), Late Triassic (230 and 211 Ma), Early Jurassic (193 Ma) and Late Jurassic (159 Ma), which primarily correspond to tectonic events from the Late Paleozoic to Early Mesozoic orogenic cycle including the Early Permian–Late Triassic subduction and collision, and the Jurassic post-orogeny spreading and collapse.

In recent years, a growing number of Late Silurian to Late Devonian granitoids were gradually found, such as the Wulanwuzhuer porphyry granite (416.7 ± 3.3 Ma) (Sun *et al.* 2009) and peraluminous monzongranite (413 ± 5 Ma) (Tan *et al.* 2011), the Adatan syenogranite (412.9 ± 2.1 Ma) (Wang 2011), the Donggou biotite monzogranite (410.2 ± 1.9 Ma) (Wang *et al.* 2004), the Akechukesai quartz diorite (407.7 ± 7.5 Ma) (Luo *et al.* 2004), the Bokelike porphyritic monzongranite (408.3 ± 5.3 Ma) (Luo *et al.* 2004), the Bayinguole gabbro (386.9 ± 2.6 Ma, 386.4 ± 3.2 Ma) (Luo *et al.* 2004), and the Kayakedengtage complex pluton of gabbro and monzonitic granite (respectively, 403.3 ± 7.2 and 394 ± 13 Ma) (Chen *et al.* 2006).

From the Late Silurian to the Late Devonian, the outcropped granitoids have almost no time gaps among them, further confirming that multiperiodic magmatic activity existed in the Qimantagh area during this period.

6.2 *Compositions of the rock*

Granitoids are genetically classified as either mantle origin (e.g., Turner *et al.* 1992; Han *et al.* 1997; Volkert *et al.* 2000), mixed origin, with various proportions of crust- and mantle-derived components (e.g., Poli and Tommasini 1991; Barbarin and Didier 1992; Wiebe 1996; Altherr *et al.* 2000; Chen *et al.* 2002; Bonin 2004) or crustal origin (e.g., Chappell and White 1992; Chappell 1999).

Based on the major elemental systematics, the Late Silurian–Late Devonian granitoids are typical of the high-K calc-alkaline, metaluminous or weakly or strongly peraluminous rocks. The lithology is mainly granodiorite and monzogranite. But from the Early Devonian, the rocks have a trend of quartz-diorite–quartz-granodiorite–monzogranite, apparently containing intermediate-basic rocks, indicating that mantle component most likely participated in the magmatic activities. Some scholars (Luo *et al.* 2004; Chen *et al.* 2006; Mo *et al.* 2007) also noted that underplating of the mantle-derived magma had happened in the study area since the Early Devonian. The origin of the high-K calc-alkaline rocks has been the subject of some studies, and two main models have been proposed to interpret their petrogenesis: (1) pure crustal melts from partial melting of mafic lower crust at relatively high pressures (e.g., Roberts and Clemens 1993; Liu *et al.* 2002) or (2) evolution result of a mixture of crustal- and mantle-derived magmas (e.g., Barbarin 1999; Ferre' and Bernard 2001; Chen *et al.* 2003; Yang *et al.* 2007). The Late Silurian granitoids may be generated by partial melting of mafic lower crust at relatively high pressures and belong to crustal origin. But from the Devonian, there are mixed origin granitoids, with various proportions of crust- and mantle-derived components.

From the REE distribution patterns and Eu anomaly, the REE distribution characteristics of crust-mantle mixed-source granites are light REE enrichment, inconspicuous Eu depletion and $\delta Eu>0.5$ (an average of 0.8 or so), and the REE distribution patterns are a right-dipping, nearly smooth type (Luo 1986; Zhao *et al.* 2008). Nevertheless, the REE distribution patterns of a crust-derived granitoid are a 'V' type curve, showing relatively obvious Eu depletion (approximately moderate to significant depletion) and relative HREE enrichment (Luo 1986). There are both 'V' type curves and smooth curves for the REE distribution in the study area. The REE distribution patterns are mainly 'V' type curves for the Late Silurian and approximately moderate to significant Eu depletion, suggesting that the Late Silurian granitoids are of crustal origin. However, the patterns are mostly an obviously smooth curve for the Devonian and weakly negative or inconspicuous Eu anomalies, especially the Early Devonian and Late Devonian, implying that the Early Devonian and Late Devonian granitoids are mainly mixed origin, although there are still some crustal source granites at the same time, especially the Middle Devonian granitoids. Obvious Eu anomalies (average 0.40) in

the Middle Devonian granitoid may be related to strong fractional crystallisation of the plagioclase during magma evolution, which is corroborated by the Middle Devonian rocks with high differentiation indices (DI) (70.56–94.68).

According to the primitive-mantle normalised spidergrams, the granitoids show similar or roughly consistent trace element characteristics of enriching in LILE (such as Rb, Th and K), HFSE (such as Zr and Hf) and depleting in Ba, Nb, Ta, Sr, P, Eu, and Ti. They also present a certain evolution trend of the orogenic belt, namely, the common enrichment of Rb, Th, Zr and Hf, significant depletion of Ti, Sr, P and Ba. As shown in the spider diagram, compared to Rb and Th, Ba is obviously depleted. The negative Ba anomalies in the granite suggest a partial melting of crustal rock (Wan 1999). The granitoids are characterized by pronounced negative Ba, Nb and Ti anomalies and enriched in LILEs and LREEs, suggesting typical crustal melts. However, these features are not always related to the crustal-derived melts and they might point to partial melting of an enriched mantle, which was metasomatized by fluids prior to melting (Hawkesworth *et al.* 1993; Rottura *et al.* 1998; Cameron *et al.* 2003). Compared to rocks from other times, the Middle Devonian granites have pronounced Ba, Sr, P and Ti depletion. This observation may be due to the strong fractional crystallisation of feldspar minerals such as potassium feldspar, plagioclase and apatite, while Ti depletion may be related to the fractional crystallisation of Ti-rich minerals such as ilmenite, sphene, and rutile during the evolution process. The Ti depletion also suggests that the magma was derived from the crust because Ti does not easily enter the melt and residue in the source. Thus, the strong Ti depletion and the relatively weak Nb and Ta depletion in the study area are due to the fractional crystallisation of ilmenite in the source. This observation is consistent with the rocks that experienced strong fractional crystallisation and belonged to highly differentiated granite, which mainly reflects the characteristics of the source.

In addition, some elemental ratios could indicate compositions of the rock. Bea *et al.* (2001) note that the Nd/Th ratio is approximately 3 for crust-derived rocks and over 15 for mantle-derived rocks. The Nd/Th ratios of the Late Silurian granitoid (0.91–3.73, average 1.97) mostly show characteristics of a crustal source. However, the Nd/Th ratios of granitoids since the Early Devonian (0.44–7.04) indicate crust and mantle mixing, which denotes an underplating of mantle magma and a change in the tectonic setting during this period. Taylor and McLennan (1985) believe that K and Rb travelled upward to the sialic layer, so they are more depleted in the mantle. Sr mainly exists in plagioclase as a substitute for Ca. As a result, high Rb/Sr ratios in the granitoids suggest a primarily upper crust source. Tischendorf (1986) also stated that the Rb/Sr ratio was an important parameter to trace the origin. The Rb/Sr ratio is <0.05 for mantle-derived magma, 0.05–0.5 for mixed crust-and-mantle magma, and over 0.5 for crust-derived magma. The Rb/Sr ratios of the Late Silurian granitoid (0.71–10.98, average 1.83) suggest a crustal reservoir as the major source, but the Rb/Sr ratios of the granitoids since the Early Devonian (0.12–22.73) indicate crust and mantle mixing in parts of the samples.

Therefore, on the whole, the Late Silurian to Late Devonian granitoids have complex composition sources. The Late Silurian granitoids are mainly crust-derived, high-K calc-alkaline peraluminous granite. However, mantle-derived compositions were involved in the magmatism starting from the Early Devonian, and the granitoids contained characteristics of a crust-mantle mixed source. Most of the Devonian granitoids are crust-mantle mixed-source, high-K calc-alkaline metaluminous and weakly peraluminous granite, and only some parts of them are crust-derived, high-K calc-alkaline peraluminous granite, especially the Middle Devonian granitoids. Due to strong crystallisation differentiation, highly fractionated granites possibly emerged in the Middle Devonian. These complex composition sources may be related to a relatively more complex tectonic environment and even its evolution process.

6.3 *Tectonic setting*

Some scholars (Bai *et al.* 2004; Wang *et al.* 2004, 2011; Sun *et al.* 2009; Tan *et al.* 2011) state that the research area was in a syn-collision tectonic environment during the Late Silurian (approximately 421–410 Ma). Zhang *et al.* (2012) firmly contend that the Qaidam continental block and the central Kunlun block were still in a state of collision in the Early Devonian (395 Ma). Other scholars (Cao *et al.* 2011; Wu *et al.* 2012) believe that the research area had been in the beginning of a syn-collision convergence environment since the Early Silurian (approximately 430 Ma), while others (Wang *et al.* 2004; Chen *et al.* 2006; Li *et al.* 2013) argue that the Qimantagh area was in a collision orogenic stage that continued until at least the Late Devonian. Zhao *et al.* (2008) contend that the Early Devonian granitoid was formed in a post-collision tectonic setting; due to the geochemical plots, parts of the granite belong to syn-collision S-type granite, so some scholars believe that it formed in an intercontinental collision orogenic process, namely, a syn-collision tectonic setting.

In recent years, research found that a continental collision phase is not conducive to the ascent of magma. Although magmatism was widely distributed during the plate period, it was very sparse. However, most of the magmatism typically occurs after, rather than before, the collision period, namely, the post-collision tectonic setting described by Liegeois (1998). In this sense, the exposed Late Silurian to Late Devonian high-K calc-alkaline granites indicate that the study area may have been in an intracontinental collision orogenic stage, during which significant amounts of post-collision high-K calc-alkaline peraluminous granite and metaluminous or weakly peraluminous granite form.

In our present study, we suggest that the regional tectonic setting during this period should belong to an intracontinental collision orogenic process, further developing post-collision granites. Moreover, additional granites emplaced in the syn-collision stage may have formed during the post-collision process, which is also confirmed in the tectonic setting discrimination diagrams (figures 7, 8). In figure 7(a), almost all the Late Silurian–Late Devonian granitoids drop into the collision setting granites and show an evolutionary tendency towards intraplate granites; in figure 7(b), parts of the granitoids drop into volcanic-arc granites (VAG), which may be related to a source that inherited the characteristics of volcanic arc; in the Rb–Y+Nb and Rb–Yb+Ta tectonic environment discrimination diagrams (figure 8), the Late Silurian–Late Devonian granitoids are also virtually all post-collision granites in the research area. Therefore, the Late Silurian–Late Devonian granitoids are post-collision granites that formed during an intracontinental collision orogeny.

In addition, the trace elements have consistent characteristics with volcanic-arc granites in a subduction setting. However, the ocean basin closed sometime before the Late Silurian (Chen *et al.* 2002; Mo *et al.* 2007; Lu *et al.* 2010; Zhang *et al.* 2010; Liu *et al.* 2012). Therefore, it is impossible that the study area was in a subduction stage in the Late Silurian–Late Devonian. The only possible explanation is that the magma source rock inherited the characteristics of a volcanic arc (Hooper *et al.* 1995; Li and Lu 1999); that is to say, the granites were derived from the partial melting of the original rocks, which were restored in the crust or the lithosphere during the subduction and collision periods in a certain tectonic setting (Liu 2000; Xiao *et al.* 2002). Li and Lui (1999) also suggested the concept of 'retarded type calc-alkaline volcanic rocks', which describes a phenomenon where the rocks show characteristics of volcanic-arc granite without the presence of a volcanic arc.

Just as Bonin *et al.* (1998) pointed out, the post-collision event started with magmatic processes still influenced by subducted crustal materials. The dominantly calc-alkaline suites show a shift from normal to high-K to very high-K associations. Source regions are composed of depleted and later enriched orogenic subcontinental lithospheric mantle, affected by dehydration melting and generating more and more K- and LILE-rich magmas. In the vicinity of intracrustal magma chambers, anatexis by incongruent melting of hydrous minerals may generate peraluminous granitoids bearing mafic enclaves. The post-collision event ends

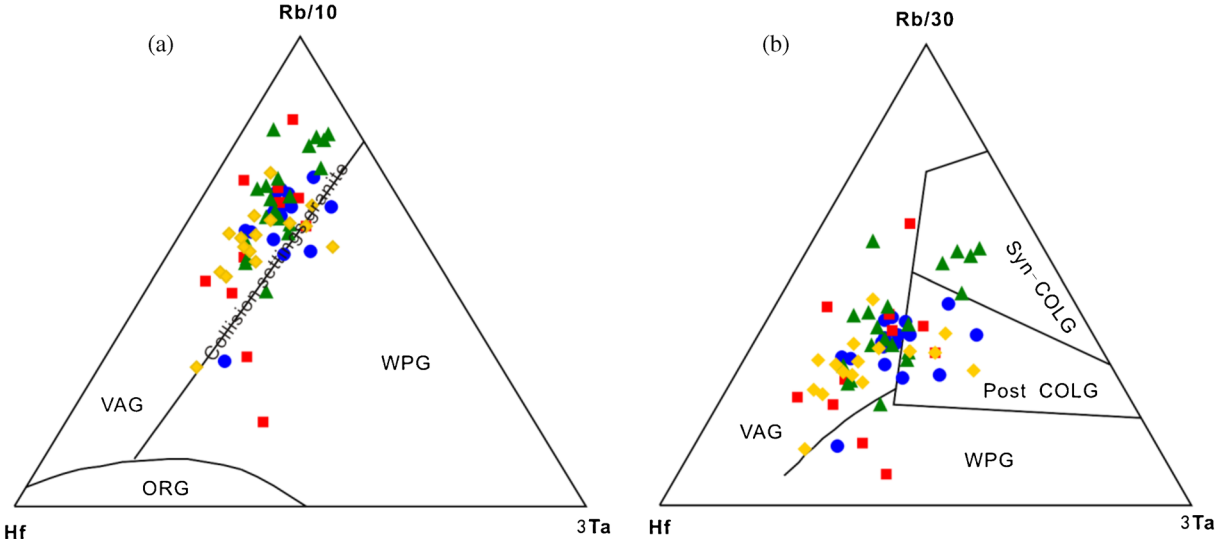

Figure 7. **(a)** Rb/10-Hf-3Ta and **(b)** Rb/30-Hf-3Ta. VAG: volcanic arc granites, ORG: ocean ridge granites, WPG: within-plate granites, Syn-COLG: syn-collision granites and Post-COLG: post-collision granites. Symbols as in figure 4(a).

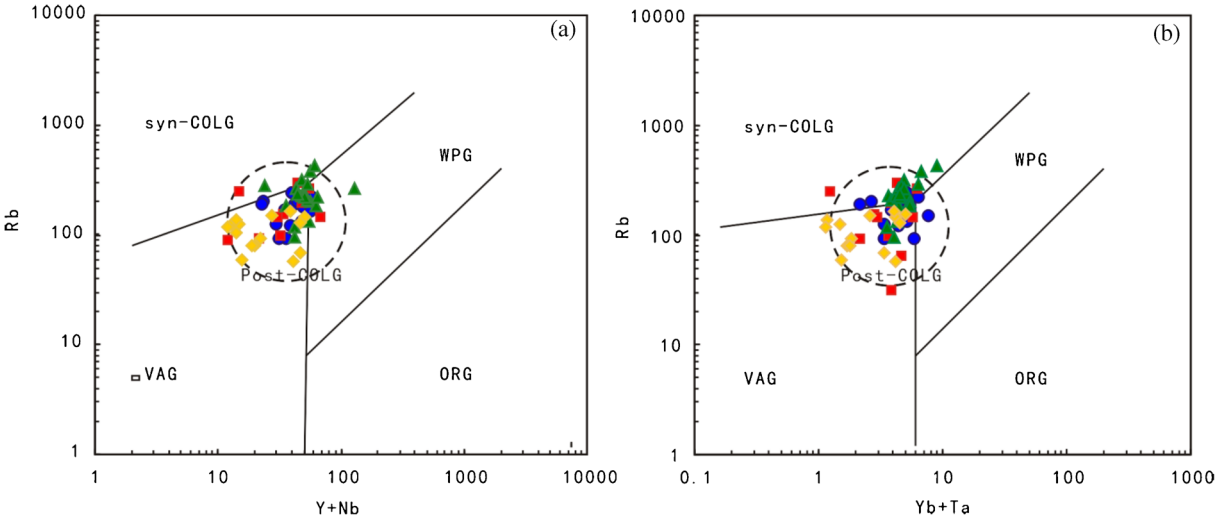

Figure 8. **(a)** Rb/10-Hf-3Ta and **(b)** Rb/30-Hf-3Ta. VAG: volcanic arc granites, ORG: ocean ridge granites, WPG: within-plate granites, Syn-COLG: syn-collision granites and Post-COLG: post-collision granites. Symbols as in figure 4(a).

with emplacement of bimodal post-orogenic. Post-collision granite suites are a case of multisource multiprocess magmatism.

Although the Late Silurian–Late Devonian granitoids are post-collision granites that formed during an intracontinental collision orogeny, according to the characteristics of major and trace elements and the rock sources, there are seemingly some differences between the Late Silurian and Devonian granites in evolution process of the tectonic setting; that is, the mechanism for the formation of the granites may have varied over time. As Xiao *et al.* (2002) suggested that the post-collision tectonic setting experienced a long and complicated process, including large-scale plate motion along the shear zone, closure, lithosphere delamination, subduction of small oceanic plates, and the formation of rifts coupled with various types of magmatism. On the R1–R2 tectonic setting discrimination diagrams (figure 9), the granitoids are associated with the orogenic environment. Although most of the granites are in the syn-collision area, they may have only been emplaced in the syn-collision stage and formed in a post-collision stretch tectonic setting. Moreover, most of the Late Devonian granites dropped into the late-orogenic stage area, indicating the end of the orogenic stage.

Therefore, the Late Silurian–Late Devonian granitoids are post-collision granites that formed during an intracontinental collision orogeny. This special tectonic setting is also in accordance with the complex composition sources.

Thus, based on the previous research results, the authors consider the evolution process of the subduction and even syn-collision have ended at least before the Late Silurian (420 Ma)

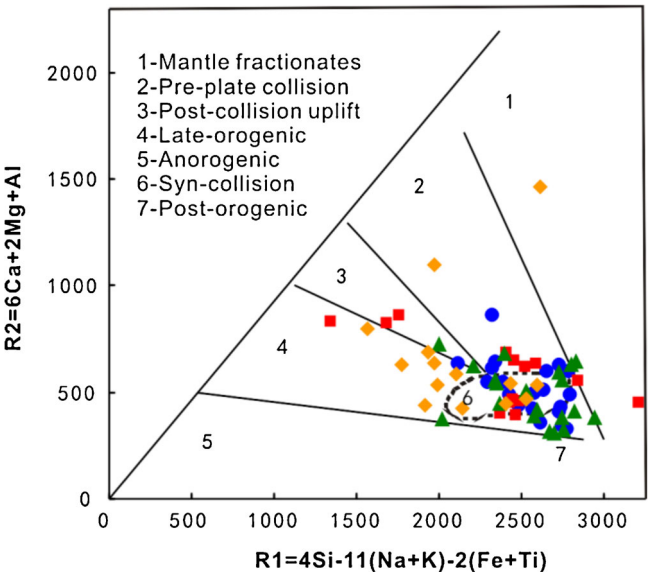

Figure 9. Plot of granites in Qimantagh area on the R1–R2 diagram of Batchelor and Bowden (1985). Symbols as in figure 4(a).

(figure 10a). The paper concludes that the 420.6 ± 2.6 Ma (sample K5, biotite monzonitic granite) and 421.2 ± 1.9 Ma (sample K46-2, potassium granite) samples were formed during a conversion period involving syn-collision extruding orogenesis progressing towards a post-collision stretch tectonic regime (420 Ma). These two samples were generated by partial melting of mafic lower crust that was restored during the subduction and collision periods (figure 10b). Next, lithosphere delamination may have occurred in the Early Devonian under a layer of thickened continental crust. This process lead to the upward gushing of mantle magma, providing a heat (heats and melts crustal

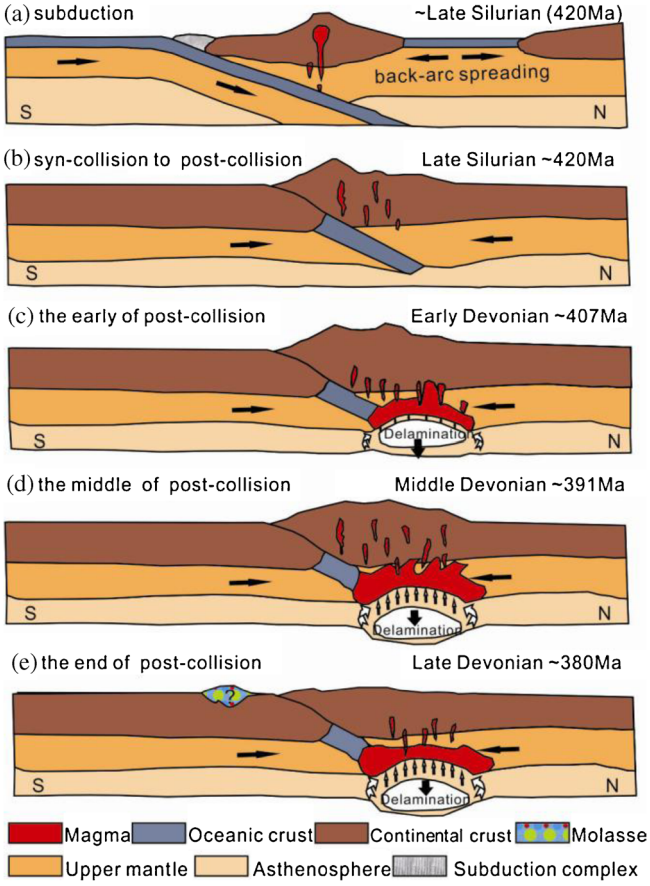

Figure 10. The Late Silurian–Late Devonian tectonic evolution model in the Qimantagh area. **(a)** The subduction and even syn-collision have ended at least before 420 Ma; **(b)** a conversion period from syn-collision extruding orogenesis to a post-collision stretch tectonic regime; **(c)** lithosphere delamination occurred under a layer of thickened continental crust; **(d)** lithosphere extension and thinning and the continued upward movement of the mantle magma, and the middle-shallow crustal rocks partially melted; **(e)** the underplating of mantle-derived magma still existed.

material) and material source (mixes the molten and mantle-derived magma that is infused into the melting crust source) and resulting in the formation of the 403.7 ± 2.9 Ma K13-1 (granodiorite) sample (figure 10c), which reflects a mixture of enriched subcontinental lithospheric mantle-derived and lower crustal-derived magmas. In this scenario, the lithospheric mantle-derived basaltic melt first mixed with granitic magma of crustal origin at depth. Then, the melts, which subsequently underwent a fractional crystallization and crustal assimilation processes, could ascend to shallower crustal levels to generate a variety of rock types ranging from diorite to granite. The trend from diorite to granite is also observed, especially the Early Devonian and Late Devonian. With the progressive lithosphere extension and thinning and the continued upward movement of the mantle magma, which provided uninterrupted heat and material sources to the crust until the Middle Devonian period, the middle-shallow crustal rocks partially melted, resulting in the formation of the 391.3±3.2 MaK21-2 granite porphyry (figure 10d), which underwent strong crystallisation differentiation, and belong to highly fractionated granites. This type of relatively loose and stretch post-collision tectonic setting lasted at least until the early Late Devonian, resulting in the formation of the 380.52 ± 0.92 Ma K36-2 (granodiorite) sample. In addition, there is a basic gabbro mass of similar age (380.3 ± 1.5 Ma) (Ren *et al.* 2012) in the same place that co-exists well with the granitoid. This observation confirms the existence of tectonic magmatic activity during this period; namely, the underplating of mantle-derived magma still existed in the Qimantagh area during the Late Devonian (380 Ma). Eventually, the development of the continental molasse in the Late Devonian marked the end of the Qimantagh area's Early Paleozoic Caledonian orogenic cycle (figure 10e).

7. Conclusions

From our study of Late Silurian–Late Devonian granitoids in the Qimantagh area of the East Kunlun orogenic belt, we arrived at the following conclusions:

- Multiperiodic magmatic activity existed in the Qimantagh area during the Late Silurian (approximately 420 Ma)–Late Devonian (approximately 380 Ma). The zircon U–Pb ages of 5 samples in the Qimantagh area are 420.6 ± 2.6 Ma (Nalingguole biotite monzogranite), 421.2 ± 1.9 Ma (Wulanwuzhuer potassium granite), 403.7 ± 2.9 Ma (Yemaquan granodiorite), 391.3 ± 3.2 Ma (Qunli granite porphyry), and 380.52 ± 0.92 Ma (Kayakedengtage granodiorite).
- The Late Silurian–Late Devonian granitoids belong to the subalkaline, high-K calc-alkaline, metaluminous or weakly or strongly peraluminous series. The rocks are right oblique types, having overall relative LREE enrichment and HREE depletion and different degrees of Eu anomalies, trending towards moderate Eu depletion at different times, and are enriched in LILE, such as Rb, Th and K, and HFSE, such as Zr and Hf, and depleted in Ba, Nb, Ta, Sr, P, Eu, and Ti.
- The Late Silurian–Late Devonian granitoids have complex composition sources. The Late Silurian granitoids are mainly crust-derived and mantle-derived material was involved in the magmatism starting from the Early Devonian, as well as the granitoid-contained characteristics of a crust-mantle mixed source. Most of the Devonian

granitoids are crust-mantle mixed-source, and only some parts of them are crust-derived, especially the Middle Devonian granitoids.

- The Late Silurian–Late Devonian granitoids were formed in a post-collision tectonic setting. Lithosphere delamination may have occurred in the Early Devonian (407 Ma), and the study area subsequently experienced an underplating of the mantle-derived magma at least until the Late Devonian (380 Ma).

Acknowledgements

The authors would like to express sincere thanks to Academician Mo Xuanxue of CUGB, Engineer Ma Zhongyuan, and Shu Xiaofeng of Third Institute of Qinghai Geological Mineral Prospecting for their encouragement and support. They also gratefully acknowledge the anonymous reviewers for their detailed reviews and constructive suggestions. Funding for this study is supported by the China Geological Survey (No. 2011-03-04-06), Found Project of the Geology and Mineral Exploration Development Authority of Qinghai Province (2013-103), and the National Natural Science Foundation of China (Nos. 41172088, 40872141 and 41072160).

References

Altherr R, Henjes-Kunst F, Langer C and Otto J 2000 Interaction between crustal-derived felsic and mantle-derived mafic magmas in the Oberkirch Pluton (European Variscides, Schwarzwald, Germany); *Contrib. Mineral. Petrol.* **137** 304–322.

Andersen T 2002 Correction of common lead in U–Pb analyses that do not report ^{204}Pb; *Chem. Geol* **192** 59–79.

Bai Y S, Chang G H, Tan S X, Ma Y M, Hao P, Suo S F, Wang J T and Bao G P 2004 Geological map of the Kulangmiqiti Region (1: 250000) Qinghai; *Geology,* pp. 147–162.

Barbarin B 1999 A review of the relationships between granitoid types, their origins and their geodynamic environments; *Lithos* **46** 605–626.

Barbarin B and Didier J 1992 Genesis and evolution of mafic microgranular enclaves through various types of interaction between coexisting felsic and mafic magmas; *Trans. Roy. Soc. Earth Sci.* **83** 145–153.

Batchelor R A and Bowden P 1985 Petrogenetic interpretation of granitoid rock series using multi-cationic parameters; *Chem. Geol* **48(1/4)** 43–55.

Bea F, Arzamastsev A, Montero P and Arzamastseva L 2001 Anomalous alkaline rocks of Soustov, Kola: Evidence of mantle-derived metasomatic fluids affecting crustal materials; *Contrib. Mineral. Petrol.* **140(5)** 554–566.

Be'dard J H 2006 A catalytic delamination-driven model for coupled genesis of Archaean crust and subcontinental lithospheric mantle; *Geochim. Cosmochim. Acta* **70** 1188–1214.

Belousova E A, Griffin W L, O'Reilly S Y and Fisher N I 2002 Igneous Zircon: Trace element composition as an indicator of source rock type; *Contrib. Mineral. Petrol.* **143** 602–622.

Bonin B 2004 Do coeval mafic and felsic magmas in post-collisional to within-plate regimes necessarily imply two contrasting, mantle and crustal, sources? A review; *Lithos* **78** 1–24.

Bonin B, Azzouni-Sekkal A, Bussy O F and Ferrag S 1998 Alkali-calcic and alkaline post-orogenic (PO) granite magmatism: Petrologic constraints and geodynamic settings; *Lithos* **45** 45–70.

Cameron B I, Walker J A, Carr M J, Patino L C, Matias O and Feigenson M D 2003 Flux versus decompression melting at stratovolcanos in southeastern Guatemala; *J. Volcanol. Geotherm. Res.* **119** 21–50.

Cao S T, Liu X K, Ma Y S, Li J Y and Ma Y L 2011 The found of the Early Silurian intrusive rock and its geological significance in Qimantagh area; *Qinghai Sci. Tech.* **5** 26–30 (in Chinese).

Cao Y Q, Luo Z H and Deng J F 1999 Paleozoic volcanic activities and tectonic evolution of the Eastern Kunlun mountains – the northern margin of the Qaidam basin; *Geol. Rev.* **45(Suppl.)** 1002–1009 (in Chinese).

Chappell B W 1999 Aluminum saturation in I- and S-type granites and the characterization of fractionated hapogranites; *Lithos* **46** 531–551.

Chappell B W and White A J R 1992 I- and S-type granites in the Lachlan Fold Belt; *Trans. Roy. Soc. Edinb. Earth Sci.* **83** 1–26.

Chen B, Jahn B M and Wei C 2002 Petrogenesis of Mesozoic granitoids in the Dabie UHP complex, central China: Trace element and Nd–Sr isotope evidence; *Lithos* **60** 67–88.

Chen B, Jahn B M and Zhai M G 2003 Sr–Nd isotopic characteristics of the Mesozoic magmatism in the Taihang–Yanshan orogen, north China craton, and implications for Archean lithosphere thinning; *J. Geol. Soc. London* **160** 963–970.

Chen H W, Luo Z H, Mo X X, Liu C D and Ke S 2005 Underplating mechanism of Triassic granite of magma mixing origin in the East Kunlun orogenic belt; *Geol. China* **32(3)** 386–395.

Chen H W, Luo Z H, Mo X X, Zhang X T, Wang J and Wang B Z 2006 SHRIMP ages of Kayakedengtage complex in the East Kunlun and their geological implications; *Acta Petrol. Mineral.* **25(1)** 25–32 (in Chinese with English abstract).

Chen N S, He L, Sun M, Wang G C and Zhang K X 2002 Precise timing of the Early Paleozoic metamorphism and thrust deformation in the Eastern Kunlun Orogen; *Chinese Sci. Bull.* **47** 628–631 (in Chinese).

Cheng Y Q 1994 *Outline of regional geology of China* (Beijing: Geol. Publ. House), pp. l–517 (in Chinese with English abstract).

Fang N Q and Liu B P 1996 Tectono-sedimentray features of the Muyinhe Formation and stratigraphic subjects concerned in southwestern Yunnan; *J. China Univ. Geosci. (Earth Sci.)* **21(1)** 11–18 (in Chinese with English abstract).

Ferre' E C and Bernard E L 2001 Geodynamic significance of early orogenic high-K crustal and mantle melts: Example of the Corsica Batholith; *Lithos* **59** 47–67.

Gao S and Jin Z M 1997 Delamination and its geodynamical significance for crust-mantle evolution; *Geol. Sci. Technol. Inform.* **16(1)** 1–9.

Guo T Z, Liu R, Chen F B, Bai X D and Li H G 2011 LA-MC-ICPMS zircon U–Pb dating of Wulanwuzhuer porphyritic syenite granite in the Qimantag Mountain of Qinghai and its geological significance; *Geol. Bull. China* **30(8)** 1203–1211 (in Chinese with English abstract).

Han B F, Wang S G, Jahn B M, Hong D W, Kagami H and Sun Y L 1997 Depleted mantle source for the Ulungur River A-type granites from North Xinjiang, China: Geochemistry and Nd–Sr isotopic evidence and implications for Phanerozoic crustal growth; *Chem. Geol* **138** 135–159.

Hawkesworth C J, Gallagher K, Herot J M and McDermott F 1993 Mantle and slab contributions in arc magmas; *Ann. Rev. Earth Planet. Sci.* **21** 175–2004.

Hooper P R, Bailey D G and Holder G A M 1995 Tertiary calc-alkaline magmatism associated with liospheric extension in the Pacific northwest; *J. Geophys. Res.* **100(B7)** 10,303–10,319.

Huang J Q, Ren J S, Jiang C F, Zhang Z M and Xu Z Q 1977 An outline of the tectonic characteristics of China; *Acta Geologica Sinica* **2** 117–135 (in Chinese with English abstract).

Huang J Q 1984 New researches on the tectonic characteristics of China; *Chinese Geol. Sci. Acad. Bull.* **9** 5–18 (in Chinese with English abstract).

Jiang C F 1992 *Opening–Closing Tectonics of Kunlun Mountains*; Geological Publishing House, Beijing.

Jiang C F 1994 From the polycyclicity theory to open-and-close tectonics; *Acta Geoscientia Sinica* **3–4** 103–112 (in Chinese with English abstract).

Jiang C F, Wang Z Q and Li J Y 2000 *Open-Close Tectonics in the Central Orogenic Belt* (Beijing: Geological Publishing House), pp. 1–154 (in Chinese with English abstract).

Li H K, Geng J Z and Hao S 2009 Research on the dating zircon U–Pb age by LA-MC-ICPMS; *Bull. Mineral. Petrol. Geochem.* **28(Suppl.)** 77 (in Chinese with English abstract).

Li W P and Lu F X 1999 New progress of the study of geologic setting for calc-alkline volcanic rocks; *Geol. Sci. Technol. Inform.* **18(2)** 15–18 (in Chinese).

Li W, Neubauer F, Liu Y J, Johann G, Ren S M, Han G Q and Liang C Y 2013 Paleozoic evolution of the Qimantagh magmatic arcs, Eastern Kunlun Mountains: Constraints from zircon dating of granitoids and modern river sands; *J. Asian Earth Sci.* **77** 183–202.

Liegeois J P 1998 Some words on the post-collisional magmatism; *Lithos* **45** 15–18.

Liu B, Ma Q C, Zhang J Y, Xiong F H, Huang J and Jiang H A 2012 Petrogenesis of Early Devonian intrusive rocks in the east part of Eastern Kunlun Orogen and implication for Early Paleozoic orogenic processes; *Acta Petrologica Sinica* **28** 1785–1807 (in Chinese with English abstract).

Liu C D, Mo X X, Luo Z H, Yu X H, Chen H W, Li S W and Zhao X 2003 Pb–Sr–Nd–O isotope characteristics of granitoids in East Kunlun Orogenic Belt; *Acta Geoscientica Sinica* **24(6)** 584–588 (in Chinese with English abstract).

Liu H T, Sun S H, Liu J M and Zhai M G 2002 The Mesozoic high-Sr granitoids in the northern marginal region of north China craton: Geochemistry and source region; *Acta Petrol. Sin.* **18** 257–274.

Liu X M 2000 Tectonic environment and the characteristics of the post-collision magmatic rocks; *Prog. Precamb. Res.* **23(2)** 121–127 (in Chinese).

Lu L, Wu Z H, Hu D G, Barosh P J, Hao S and Zhou C J 2010 Zircon U–Pb ages for rhyolite of the Maoniushan Formation and its tectonic significance in the East Kunlun Mountains; *Acta Petrologica Sinica* **26** 1150–1158 (in Chinese with English abstract).

Luo T C 1986 The significance of studying rare earth element geochemistry in granite type; *Geol. Sci. Technol. Inform.* **2** 046 (in Chinese).

Luo Z H, Mo X X, Wang J H and Zhao Z D 2004 The mantle-crust interactions during continental collision process of the Plateau and their effects on the formation of mineral resources and oil-gas pools; In: Uplifting of Tibetan Plateau with its environmental effects (eds) Zheng D and Yao T D (Beijing: Science Press), pp. 117–163.

Middlemost E A K 1985 *Magmas and Magmatic Rocks* (London: Longman), pp. 1–266.

Mo X X, Luo Z H, Deng J F, Yu X H, Liu C D, Chen H W, Yuan W M and Liu Y H 2007 Granitoids and crustal growth in the East-Kunlun Orogenic Belt; *Geol. J. China Universities* **13(3)** 403–414 (in Chinese with English abstract).

Pan G T, Li X Z, Wang L Q, Ding J and Chen Z L 2002 Preliminary division of tectonic units of the Qinghai–Tibet Plateau and its adjacent regions; *Geol. Bull. China* **21(11)** 701–707 (in Chinese with English abstract).

Pan Y S, Zhou W M, Xu R H, Wang A D, Zhang Y Q, Xie Y W, Chen T E and Luo H 1996 Geological characteristics and evolution of the Kunlun Mountain region during the early Paleozoic; *Sci. China (Series D: Earth Sci.)* **4** 302–307 (in Chinese with English abstract).

Peccerillo R and Taylor S R 1976 Geochemistry of eocene calc-alkaline volcanic rocks from the Kastamonu area, northern Turkey; *Contrib. Mineral. Petrol.* **58** 63–81.

Poli G E and Tommasini S 1991 Model for the origin and significance of microgranular enclaves in calc-alkaline granitoids; *J. Petrol.* **32** 657–666.

Qu G S, Chen J, Chen X L, Zhang X L, Li T, Yin J P and Zhou H Q 1994 Intraplate deformation in the front of the West Kunlun Pamir Areuate Orogenic Belt and the southwest Tarim Foreland Basin; *Geol. Rev.* **44(4)** 419–429 (in Chinese with English abstract).

Ren E F, Zhang G L, Qiu W, Li H X and Sun Z H 2012 Characteristics of geochemistry and tectonic significance of Caledonian granite in the Maerzheng region in the south area of East Kunlun; *Geosciences* **26(1)** 36–44 (in Chinese with English abstract).

Roberts M P and Clemens J D 1993 Origin of high-potassium, calc-alkaline, I-type granitoids; *Geology* **21** 825–828.

Rottura A, Bargossi G M, Caggianelli A, Del Moro A, Visona D and Tranne C A 1998 Origin and significance of the Permian high-K calc-alkaline magmatism in the central-eastern southern Alps, Italy; *Lithos* **45** 329–348.

Sun F Y, Li B L, Ding Q F, Zhao J W, Pan T, Yu X F, Wang L, Chen G J and Ding Z J 2009 Prospecting Problems: Studies of East Kunlun Metallogenic Belt; *Geol. Survey Report China Geol. Survey,* pp. 14–17 (in Chinese).

Sun S S and McDonough W F 1989 Chemical and isotopic systematics of oceanic basalts: Implications for mantle composition and processes; *Geol. Soc. London, Spec. Publ.* **42** 313–345.

Tan S X, Guo T Z, Dong J S, Chang Y Y and Ma W 2011 Geological characteristics and significance of the peraluminous granite in Late Silurian epoch in Wulanrvuzhuer region of Qinghai; *J. Qinghai University (Nature Sci.)* **29(1)** 36–43 (in Chinese with English abstract).

Taylor S R and McLennan S M 1985 *The Continental Crust: Its Composition and Evolution*; Blackwell, Cambridge.

Tischendorf G 1986 The rock classification of granites; *Foreign Geol. Sci. Tech.* **7** 25–33 (in Chinese).

Turner S P, Foden J D and Morrison R S 1992 Derivation of some A-type magmas by fractionation of basaltic magma: An example from the Padthaway Ridge, South Australia; *Lithos* **28** 151–179.

Volkert R A, Feigenson M D, Patino L C, Delaney J S and Drake A A Jr 2000 Sr and Nd isotopic compositions, age and petrogenesis of A-type granitoids of the Vernon

Supersuite, New Jersey Highlands, USA; *Lithos* **50** 325–347.

Wan Y S 1999 Ba anomaly and its geochemical significance; *Continental Dynamics* **4(1)** 84–87.

Wang B Z 2011 The study and investigation on the assembly and coupling petrotectonic assemblage during Paleozoic–Mesozoic period at Qimantage geological corridor domain; *China Univ. Geosci.*, PhD thesis, pp. 171–133 (in Chinese with English abstract).

Wang B Z, Wang J, Ye Z F, Song T Z, Xue N, Li Y, Suo Y X and Ma Y S 2004 Geological map of the Bukedabanfeng region (1: 250000) Qinghai; *Geology,* pp. 109–128.

Wang H Z, Liu B P and Li S T 1990 Geotectonic units and tectonic development of China and adjacent regions; In: Selected Works of Wang Hongzhen 2005 (Beijing: Sci. Press), pp. 359–382 (in Chinese with English abstract).

Wiebe R A 1996 Mafic-silicic layered intrusions: The role of basaltic injections on magmatic processes and evolution of silicic magma chambers; *Trans. R. Soc. Edinb. Earth Sci.* **87** 233–242.

Wu S F, Chen L B, Ren W K, Zhang H Q, Wang S H and Ding C W 2012 Discovery of rapakivite grantite and its geological implication in Qimantage; *J. Qinghai University (Natural Sci. Edn)* **30(5)** 49–54 (in Chinese with English abstract).

Xiao Q H, Deng J F and Ma D Q *et al.* 2002 *The Ways of Investigation on Granitoids* (Beijing: Geological Publishing House), pp. 1–294.

Xiao X C, Li T D, Li G C, Gao Y L and Xu Z Q 1990 Tectonic evolution of the Qinghai–Xizang (Tibet) Plateau; *Chinese Geol. Sci. Acad. Bull.* **20** 123–125 (in Chinese with English abstract).

Yang J H, Fu Y, Wu F Y, Wilde S A, Xie L W, Yang Y H and Liu X M 2007 Tracing magma mixing in granite genesis: *In situ* U–Pb dating and Hf-isotope analysis of zircons; *Contrib. Mineral. Petrol.* **153** 177–190.

Yang J S, Shi R D, Wu C L, Wang X B and Paul T R 2009 Dur'ngoi Ophiolite in East Kunlun, Northeast Tibetan Plateau: Evidence for Paleo–Tethyan Suture in northwest China; *J. Earth Sci.* **20** 303–330 (in Chinese with English abstract).

Yang K M 1994 The formation and evolution of the western Kunlun continental margin; *Geol. Rev.* **40(1)** 9–18 (in Chinese with English abstract).

Yin H F and Zhang K X 1997 Several characteristics of the East Kunlun belt; *J. China Univ. Geosci. (Earth Sci.)* **22(4)** 339–342 (in Chinese with English abstract).

Yin H F and Zhang K X 1998 Evolution and characteristics of the central orogenic belt; *Earth Sci.* **23** 437–442 (in Chinese with English abstract).

Yin H F, Wu S B and Du Y S 1999 South China defined as part of Tethyan Archipelagic Ocean System; *J. China Univ. Geosci. (Earth Sci.)* **24** 1–12 (in Chinese with English abstract).

Yuan W M, Mo X X, Yu X H and Luo Z H 2000 Geological records of the regional tectonic environments during the Indo-Chinese period within granites in the East-Kunlun; *Geol. Rev.* **46(2)** 203–211 (in Chinese with English abstract).

Zhang A K, Liu G L, Mo X X, Liu J P, Zhang W Q, Chen H F and Li Y P 2012 Relationship between tectonic settings and metallo genesis of Late Paleozoic–Early Mesozoic intrusive rock in Qimantage, Qinghai Province; *Northwestern Geol.* **45(1)** 9–19 (in Chinese with English abstract).

Zhang Y L, Hu D G, Shi Y R and Lu L 2010 SHIRMP zircon U–Pb ages and tectonic significance of Maoniushan Formation volcanic rocks in East Kunlun orogenic belt, China; *Geol. Bull. China* **29** 1614–1618 (in Chinese with English abstract).

Zhao Z M, Ma H D, Wang B Z, Bai Y S, Li R S and Ji W H 2008 The evidence of intrusive rocks about collision-orogeny during Early Devonian in Eastern Kunlun area; *Geol. Rev.* **54(1)** 47–56 (in Chinese with English abstract).

Zhong Y F, Ma C Q and She Z B 2006 Geochemical characteristics of Zircon and its applications in geosciences; *Geol. Sci. Technol. Inform.* **25(1)** 27–40 (in Chinese with English abstract).

Zhu Y H, Lin Q X, Jia C X and Wang CG 2005 Early Paleozoic volcanic zircon SHRIMP age and its geological significance of East Kunlun orogenic belt; *China Sci. (Series D: Earth Sci.)* **35** 1112–1119 (in Chinese with English abstract).

Zhu Y H, Zhang K X, Yuan P, Chen N S, Wang G C and Hou G J 1999 Determination of different ophiolitic belts in eastern Kunlun orogenic zone and their tectonic significance; *Earth Sci.* **24** 134–138 (in Chinese with English abstract).

MS received 15 May 2014; revised 1 September 2014; accepted 2 September 2014